Grenville-age continental arc magmatism and crustal evolution in central Dronning Maud Land (East Antarctica): Zircon geochronological and Hf-O isotopic evidence

Cheng-Cheng Wang[a*], Joachim Jacobs[a], Marlina A. Elburg[b], Andreas Läufer[c], Robert J. Thomas[d], Synnøve Elvevold[e]

[a] Department of Earth Science, University of Bergen, PB7803, N-5020 Bergen, Norway
Cheng-Cheng.Wang@uib.no

[b] Department of Geology, University of Johannesburg, Auckland Park 2006, Johannesburg, South Africa

[c] Federal Institute for Geosciences and Natural Resources (BGR), Stilleweg 2, 30655, Hannover, Germany

[d] Council for Geoscience, 3 Oos Street, Bellville, 7535, Cape Town, South Africa

[e] Norwegian Polar Institute, N-9296 Tromsø, Norway

* Corresponding author

Declarations of interest: none

Abstract

This study focusses on the Grenville-age Maud Belt in Dronning Maud Land (DML), East Antarctica, which was located at the margin of the Proto-Kalahari Craton during the assembly of Rodinia. We present new U-Pb zircon ages and Hf-O isotope analyses of mafic and granitic gneisses exposed in the Orvin-Wohlthat Mountains and Gjelsvikfjella, central DML (cDML). The geochronological data indicate continuous magmatic activity from 1160 to 1070 Ma which culminated at 1110–1090 Ma, followed by high-grade metamorphism between 1080 and 1030 Ma. The majority of zircons from the Orvin-Wohlthat Mountains exhibit radiogenic Hf isotopic compositions corresponding to suprachondritic ε_{Hf} (t) values and Mesoproterozoic model ages, indicating crystallization from predominantly juvenile magmas. However, the involvement of ancient sedimentary material, which were most likely derived from the adjacent Proto-Kalahari Craton, is revealed by a few samples with negative to neutral ε_{Hf} (t) and significantly elevated $\delta^{18}O$ values (8–10‰). Samples from further west, in Gjelsvikfjella have more mantle-like zircon O isotopic compositions and late Paleoproterozoic Hf model ages, indicating the incorporation of ancient, previously mantle-derived continental crust. The rocks in cDML, thus define part of an extensive Mesoproterozoic magmatic arc with subduction under the Proto-Kalahari margin. This involved significant growth of new continental crust, possibly related to slab retreat, accompanied by subordinate recycling of older crustal components. The Maud Belt has been correlated with the 1250–1030 Ma Natal Belt in southern Africa, which lay to the west in the context of Gondwana, although this assertion has recently been questioned. Our study supports the latter view in demonstrating that the continental arc magmatism in the Maud Belt appears to be temporally and tectonically unconnected to the accretion of (slightly older) juvenile oceanic islands in the Natal Belt, which, in contrast to the Maud Belt, show subduction polarity away from the craton. We thus speculate that the Namaqua-Natal to Maud Belt contact (exposed in the Heimefront Shear Zone) may represent a changed tectonic environment from arc/continent-continent collision to slightly younger continental margin orogenesis at the westernmost termination of this part of the global Grenville Orogen. The Maud Belt marks the beginning of a major, long-lived accretionary Andean-type tectonic regime on the eastern margin of Proto-Kalahari related to the extroversion of Rodinia during almost the entire Neoproterozoic and culminating in the formation of Gondwana.

Key words:

U-Pb-Hf-O; Maud Belt; crustal evolution; Rodinia; Mesoproterozoic

1. Introduction

Earth's Grenville-age orogenic belts record the assembly of the supercontinent Rodinia at the end of the Mesoproterozoic. This involved major accretionary and collisional events from 1245 Ma to 980 Ma and eventual tectonic stabilization of Rodinia after 1090 Ma (e.g. Li et al., 2008; Rivers, 2009; Hynes and Rivers, 2010; McLelland et al., 2010). The Grenville Orogen itself represents a major Himalaya-type collisional belt, mainly exposed along the eastern margin of North America (Laurentia). Although there is no consensus as to the restoration of the continental fragments enveloping Laurentia in reconstructed configurations of Rodinia (e.g. Weil et al., 1998; Dalziel et al., 2000; Pisarevsky et al., 2003; Torsvik, 2003; Li et al., 2008; Johansson, 2009; Merdith et al., 2017), combined geological and paleomagnetic data show that the collision counterparts to Laurentia may include Amazonia (Cawood and Pisarevsky, 2017), Rio de la Plata (Gaucher et al., 2011), Baltica (Bingen et al. 2008; Bingen and Viola, 2018) and Proto-Kalahari (Dalziel et al., 2000; Jacobs et al., 2003a, 2008b; Loewy et al., 2011; Swanson-Hysell et al., 2015). Whatever configutaion holds true, following amalgamation, exterior ocean basins locally evolved into accretionary orogens around parts of the periphery of Rodinia (e.g. Murphy and Nance, 2005). The subduction and convergence of these encircling orogens may have triggered the development of rifting and break-up of Rodinia at 800–750 Ma (Cawood et al., 2016). Some of the rifted continental fragments subsequently collided along the East Africa-Antarctic Orogen (EAAO) to form Gondwana during Pan-African times between ~650 and 500 Ma (Stern et al., 1994; Jacobs and Thomas, 2004).

During the assembly of Rodinia, subduction zones with different subduction polarities developed at the periphery of the Proto-Kalahari Craton, giving rise to several tectonic subdomains within the larger Grenville Orogen (e.g. Thomas et al., 1994; Jacobs et al., 2008a; Oriolo and Becker, 2018), including the Namaqua-Natal Belt in southern Africa and the Maud Belt in East Antarctica (Fig. 1). The Natal Belt was formed by a long-term accretion of island arcs and final indentation of Proto-Kalahari into Laurentia (Jacobs et al., 1993, 2003a; Mendonidis and Thomas, 2019). The Maud Belt was initially regarded as the lateral continuation of the Namaqua-Natal Belt (Fig.1a; Groenewald et al., 1995; Jacobs et al., 2003). However, recent studies proposed that they appear to be distinct with respect to subduction polarity and the timing of tectono-thermal events (Bisnath et al., 2006; Grantham et al., 2011; Mendonidis et al., 2015). Thus, the orogenic history of the Maud Belt and its correlation with the Natal Belt, remains uncertain (e.g. Groenewald et al., 1995; Bauer et al., 2003a; Paulsson and Austrheim, 2003; Grosch et al., 2007, 2015; Marschall et al., 2013).

The nature and geodynamic evolution of an orogenic belt is reflected in its history of crustal growth and recycling. During continent-continent collisional orogenesis the dominant magmatism generally reworks older crust with only minor amounts of juvenile crust produced. By contrast, subduction-related orogenic systems (island arc accretion and continental arc) usually involve progressive addition of mantle-derived (juvenile) magmas during continuous subduction of oceanic slabs (Condie, 2005; Cawood et al., 2009; Collins et al., 2011; Ducea et al., 2015; Hagen-Peter and Cottle, 2018; Spencer et al., 2019). Lu-Hf and O isotopic tracing of zircon is a well-established and powerful tool to identify the juvenile and reworked components in magmatic systems (e.g. Valley, 2003; Hawkesworth and Kemp, 2006; Kemp et al., 2007). The Hf isotopic signature reflects the relative contributions of depleted mantle and recycled continent crust, which have differing Lu/Hf ratios, and thereby develop distinct $^{176}Hf/^{177}Hf$ ratios over time. The O isotopic composition of zircons crystallized from mantle and mantle-derived magmas is assumed to be uniform (5.3 ± 0.6‰, 2σ; Valley et al., 1998). Any positive deviation of $\delta^{18}O$ value from this benchmark is interpreted to be caused by contamination by supracrustal material, which tends to have enriched heavy O isotope values. Accordingly, along with U-Pb dating, Hf-O isotopic composition in zircon provides valuable information on crustal and mantle processes involved in the generation of source rocks and parent magmas.

The unravelling of the Grenville-age history of the Maud Belt is rendered extremely difficult due to later intense high-grade tectono-metamorphic overprinting in Late Neoproterozoic/Early Palaeozoic ("Pan-African") times during Gondwana assembly (Fig.1b). Because of this, previous studies have mainly focussed on this aspect of the Maud Belt. Consequently, geochronological and isotopic investigations that target the Grenville-age history are currently sparse and it is this gap in our knowledge that this paper seeks to redress, by focussing on a portion of the Maud Belt in central Dronning Maud Land (cDML, Fig. 2). In order to constrain the timing and source composition of Mesoproterozoic magmatism in cDML, an integrated zircon U-Pb dating and Hf-O isotopic study was conducted on a series of samples from the Orvin-Wohlthat Mountains and Gjelsvikfjella. The results allow us to evaluate the role of crustal growth and recycling, recognize and characterize the main Grenville-age orogenic events, and arrive at a better understanding of the geodynamic evolution of orogenic belts along the margin of the Proto-Kalahari Craton during the assembly of Rodinia.

2. Geological background: the Maud Belt

Dronning Maud Land (DML), in the South Atlantic-Indian Ocean sector of East Antarctica, comprises three main geological domains: a) the Grunehogna Craton, which represents an Archaean fragment of the Proto-Kalahari Craton (Groenewald et al., 1995; Jones et al., 2003); b) the approximately 1000 km long Grenville-age (ca. 1100 Ma) Maud Belt that relates to the amalgamation of the supercontinent Rodinia, and c) the Tonian Oceanic Arc Super Terrane (TOAST) in south-eastern and eastern DML that probably evolved outside Rodinia and was only later amalgamated to East Antarctica during Gondwana assembly (Jacobs et al., 2015, 2017) (Fig. 2). The use of the term "Proto-Kalahari Craton" in this paper follows the definition proposed by Jacobs et al. (2008), referring to the Archean-Paleoproterozoic core before Mesoproterozoic accretion produced the (full) Kalahari Craton.

The Maud Belt was first described by Groenewald et al. (1995), referring to a Mesoproterozoic orogenic mobile belt recognised at H.U. Sverdrupfjella, Kirwanveggen and Heimefrontfjella in western DML (Fig. 2). Similar Grenville-age rocks were subsequently identified across large parts of western and central DML including Gjelsvikfjella, the Mühlig-Hofmann-Gebirge and the Orvin-Wohlthat Mountains (Jacobs et al., 1998, 2003a, b; Paulsson and Austrheim, 2003; Bisnath et al., 2006; Baba et al., 2015) (Fig. 2). The Ulvetanna Lineament separates Gjelsvikfella and the Mühlig-Hofmann-Gebirge in the west from the Orvin-Wohlthat mountains in the east (Fig. 2). The eastern extent of the Maud Belt (and easternmost Kalahari) coincides with the Forster Magnetic Anomaly (Fig. 2), east of which younger rocks (990-900 Ma) of the Tonian Oceanic Arc Super Terrane (TOAST) are juxtaposed (Jacobs et al., 2015).

The Maud Belt, together with the Namaqua-Natal Belt in southern Africa, the Nampula Complex in northern Mozambique, the Falkland microplate and the Haag Nunatak block, has been restored along the margin of the Kalahari Craton in Rodinia and Gondwana reconstructions (Fig. 1, Groenewald et al., 1995; Grantham et al., 1997; Thomas et al., 2000; Jacobs and Thomas, 2004; Manhica et al., 2001). The Namaqua-Natal-Maud belt was initially considered as a single continuous orogen, formed by the accretion of island arcs on to the margin of Proto-Kalahari during the assembly of Rodinia. Recently, however, the Natal-Maud correlation has been questioned. Bisnath et al. (2006) pointed out that the two areas appear to have different subduction polarities and independent tectonic histories until high-grade metamorphism affected both belts at 1090–1070 Ma. Mendonidis et al. (2016) noted that the Natal belt has a significantly older history (> ca. 1200 Ma) than most of the Maud belt (ca. 1150 Ma). The exception to this is the granulite facies Vardeklettane Terrane in Heimefrontfjella, westernmost DML (Fig. 2, e.g. Bauer et al., 2003c, 2009), which, alone in East Antarctica, probably correlates with the Margate Terrane in Natal.

The tectonic boundary between the Vardeklettane Terrane (i.e. the Natal belt) and the rest of the Maud belt has been identified as the major Heimefront Shear Zone (Fig. 2, Jacobs et al., 1996). Furthermore, this structure forms the boundary between essentially pristine Mesoproterozoic crust in the west (Natal) and crust in the east (Maud), which was pervasively reworked in late Neoproterozoic-Cambrian times during the assembly of Gondwana. Thus, the Maud Belt can be defined as Stenian crust in DML with extensive late-Neoproterozoic/early Paleozoic reworking (Jacobs and Thomas, 2004), bounded in the west by the Heimefront Shear Zone and in the east by the major structure associated with the Forster Magnetic Anomaly (Fig. 2).

The basement rocks in the Maud Belt are dominated by Grenville-age (meta-) supracrustal and intrusive rocks formed from 1170 to 1090 Ma, followed by 1090–1050 Ma A-type granitic sheets and plutons (Arndt et al., 1991; Harris, 1999; Jackson, 1999; Bauer et al., 2003a, b; Jacobs et al., 2003a, b, 2009; Paulsson and Austrheim 2003; Board et al., 2005; Bisnath et al., 2006; Grantham et al., 2011). The emplacement of these A-type intrusions was accompanied by amphibolite- to granulite-facies metamorphism, which has been recognized from various parts of the Maud Belt (Arndt et al., 1991; Harris, 1999; Jackson, 1999; Jacobs et al., 1998; 2003a; Board et al., 2005; Bisnath et al., 2006; Marschall et al., 2013). Syn-tectonic magmatism and metamorphism were linked to convergent tectonics related either to continent-continent and/or arc-continent collision. Pre-tectonic magmatic rocks emplaced between 1170–1120 Ma are composed of granitic gneisses and subordinate mafic rocks with a common geochemical affinity to subduction-related volcanic arc rocks (e.g. Jacobs et al., 1999; Paulsson and Austrheim, 2003; Bisnath et al., 2006; Grantham et al., 2011), of which 1140–1130 Ma banded felsic and mafic gneisses were interpreted as bimodal metavolcanic rocks (Grantham, 1992; Jacobs et al., 1998; Mikhalsky and Jacobs, 2004). Most of these rocks in Heimefrontfjella, Kirwanveggen and cDML have depleted Nd isotopic compositions with Mesoproterozoic to late Paleoproterozoic model ages (1.7–1.4 Ga), indicating a relatively juvenile source composition (Arndt et al., 1991; Moyes, 1993; Jacobs et al., 1998; Wareham et al., 1998; Harris, 1999; Grantham et al., 2001). However, Paleoproterozoic-Archaean Nd model ages from H.U. Sverdrupfjella and Heimefrontfjella imply the involvement of older crust in parts of the Maud Belt (Arndt et al., 1991; Wareham et al., 1998; Grosch et al., 2007). Whether these magmas were formed along the continental margin of Proto-Kalahari or in a Rodinia-distant oceanic arc, remains ambiguous and controversial (Arndt et al., 1991; Jacobs et al., 1993, 2008; Groenewald et al., 1995; Bauer et al., 2003a; Paulsson and Austrheim, 2003; Mikhalsky and Jacobs, 2004; Grosch et al., 2007, 2015; Grantham et al., 2011). Some studies opine that the parts of the Maud Belt represent juvenile island arcs that accreted onto the Proto-Kalahari Craton margin (Groenewald et al., 1995; Bauer et al., 2003a; Grantham et al., 2011). In contrast, a continental arc setting has been supported by other studies (Frimmel, 2004; Bisnath et al., 2006; Grosch et al., 2007; Marschall et al., 2013).

Crustal components of 1.2 –1.0 Ga are also preserved in the Grunehogna Craton in western DML to the northwest of the Maud Belt (Fig. 2). The late Mesoproterozoic Ritscherflya Supergroup comprises a sedimentary sequence recording the erosional remnants of Grenville-age rocks close-by (e.g. Marschall et al., 2013). The sedimentary rocks are intruded by (ultra-) mafic and felsic intrusions (Wolmarans and Kent, 1982; Krynauw et al., 1988), which were dated at ca. 1.1 Ga (Peters et al., 1991; Moyes et al., 1995; Hanson et al., 2004).

3. Samples and analytical methods

The samples for the present study were collected during three field seasons between 1995 and 2002 with the aim of elucidating the Mesoproterozoic history of this part of cDML. Because the rocks were subject to pervasive intense Neoproterozoic-Cambrian ("Pan-African") tectono-thermal reworking and magmatism, the sampling was focused on a variety of specific lithotypes (mainly orthogneisses of various compositions). Detailed structural and intrusive relations between the lithotypes cannot be ascertained because the original relationships are totally obscured by the intense, polyphase tectonism to which they were subjected some 500 Ma after their formation. The localities for the analysed samples are marked on Fig. 2. Fifteen samples from the Orvin-Wohlthat Mountains, including granitic and mafic gneisses as well as one paragneiss, were selected for SHRIMP U-Pb dating, Lu-Hf and O isotopic investigations. In addition, six samples from Gjelsvikfjella, some 200 km west of the Orvin-Wohlthat Mountains, which had previously been U-Pb zircon dated (Jacobs et al., 2003a, 2008), were analysed for their Hf-O isotopic composition for comparison. Zircon concentrates, mount preparation, optical (reflected and transmitted light) and cathodoluminescence (CL) imaging were completed before analysis and guided the selection of the analysed spots. U-Pb, Lu-Hf and O isotopic analyses were performed on the same spot or from the same growth domain. In some cases, Lu-Hf analyses were not possible due to the necessity to use a large beam size (50 μm).

3.1 SHRIMP U-Pb dating

Twelve samples were analysed using the Sensitive High Resolution Ion Microprobe (SHRIMP) at the IBERSIMS laboratory, University of Granada, Spain and three samples (J1759, J1772, J1792) were analysed at the John de Laeter Centre, Curtin University, Australia. For details of methodology and analytical conditions see Supplementary file B of Jacobs et al. (2017) and Jacobs et al. (2008b), respectively. If common lead concentrations are low, we report uncorrected ages, otherwise we report common lead-corrected ages. Weighted mean ages and group concordant ages are calculated with Isoplot (Version 4.15; Ludwig, 2011). All errors are reported at the 2σ-level.

3.2 O-isotope system determination

Oxygen isotope ratios of zircon grains that were previously analysed for their U–Pb ages were measured using a CAMECA IMS-1280 instrument at the Swedish Museum of Natural History, Stockholm (Sweden), as well as at the IBERSIMS SHRIMP-IIe/mc facility in Granada (Spain). Prior to ion microprobe analysis, the U-Pb analysis spots were removed from the zircons by polishing followed by recoating with ~30 nm gold.

Oxygen isotope ratios of zircon grains were measured using the CAMECA IMS-1280 multicollector ion microprobe at the NordSIM Laboratory, Department of Geosciences, Swedish Museum of Natural History, Stockholm, Sweden. The analysis was performed with a c. 2 nA Cs^+ primary ion beam together with a normal incidence, low-energy, electron gun for charge compensation, medium field magnification (c. 80 ×) and two Faraday detectors (channels L'2 and H'2) at a common mass resolution of c. 2500. Measurements were performed in pre-programmed chain-analysis mode with automatic field aperture and entrance slit centring on the ^{16}O signal. The magnetic field was locked using nuclear magnetic resonance regulation for the entire analytical session. Each data-acquisition run comprised a 20 μm × 20 μm pre-sputter to remove the Au layer, followed by the centring steps and 64 s of data integration performed using a non-rastered, c.10 μm spot. Field aperture centring values were found to be well within those for which no bias has been observed during tests on standard mounts (Whitehouse & Nemchin 2009). All unknowns were analysed in 6 sessions, with every set of six unknowns bracketed by two analyses of Geostandard zircon. Detailed data processing and results are found in Supplementary File B. In session 1 and 2, the reference zircon standard is TEM2 and measured isotopic ratios were normalized to a $\delta^{18}O$ value of +8.20‰ (Black et al., 2004) (SMOW). In session 3, measured isotopic ratios were normalized to a $\delta^{18}O$ value of +9.86‰ (Wiedenbeck et al. 2004) (SMOW) for the reference zircon 91500. In session 4, 5 and 6, the reference standards are FC1 and CZ3 respectively, and measured isotopic ratios were normalized to a $\delta^{18}O$ value of +5.07‰ (SMOW) for the former and a $\delta^{18}O$ value of +14.16‰ for the latter. The values of these two standards are obtained by running them as unknowns with standard 91500. External reproducibility of 0.12–0.22‰ (SD) during the six sessions, based on the standard measurements, was propagated onto the internal precision to yield the overall uncertainty for each analysis.

Three samples (J1690, J1693, J1851) were analysed on the IBERSIMS SHRIMP_IIe/mc, following the procedure as described in Montero et al. (2017): the SHRIMP primary ion optics was set with a 120 μm Kohler aperture to produce a ~18 μm diameter spot on the mount surface. The Cs gun was set to yield a ~8 nA Cs^+ beam. The e-gun to neutralize Cs ions on non-conductive material was set to an intensity of about 1 μA. Spots to be analysed were pre-sputtered for about 5 minutes before measurements. During this time, the secondary beam and the e-gun were fully optimized to maximize the ^{16}O signal. Measurements were done in 2 sets of 10 scans each. The scans were of 10 seconds each so that the total data collection time was 200 seconds per spot. The electron-induced secondary ion emission background was recorded during 10 s before and after each set and subtracted from the ^{18}O and ^{16}O counts. TEM2 was used as the standard, with zircon measured every three unknowns and cross-checked against the 91500 zircon every 20 unknowns. The reproducibility of the standards was excellent: $\delta^{18}O = 8.20 \pm 0.30$ (2SD) for the TEM2 and $\delta^{18}O = 10.05 \pm 0.25$ (2SD) for the 91500 respectively. Data reduction was done with the POXY program developed by P. Lanc and P. Holden at the Australian National University.

3.3 Lu-Hf isotope system determination

Lu-Hf isotopes were measured at the University of Johannesburg, using an ASI Resonetics 193 nm Excimer laser ablation system coupled to a Nu Plasma II multi-collector ICPMS. Ablations were done using a 50–70 μm diameter spot, at an ablation rate of 7 Hz and an energy density of 6 J/cm^2. Prior to ablation the area was cleaned with two laser shots, and after ten seconds of decay time, the background was measured for twenty-five seconds. The signal was collected for 75 seconds during ablation. During the analytical session, accuracy and external reproducibility of the method was verified by repeated analyses of reference zircon Mud Tank, Temora2 and LV-11, which yielded $^{176}Hf/^{177}Hf$ of 0.282490 ±0.000036 (2SD, n = 56), 0.282684 ±0.000054 (2SD, n = 59), and 0.282845 ±0.000076 (2SD, n = 46), respectively. These ratios are well within the zircon reference data from Woodhead and Hergt (2005) and Heinonen et al. (2010).

For calculation of the epsilon Hf, the chondritic uniform reservoir (CHUR) was used as recommended by Bouvier et al. (2008; $^{176}Lu/^{177}Hf$ and $^{176}Hf/^{177}Hf$ of 0.0336 and 0.282785, respectively), and a decay constant of 1.867×10^{-11} (Scherer et al., 2001; Söderlund et al., 2004). Calculation of model ages is based on the depleted mantle source values of Griffin et al. (2000) with present-day $^{176}Hf/^{177}Hf$ = 0.28325 and $^{176}Lu/^{177}Hf$ = 0.0384. For granitic samples, the model ages are calculated using $^{176}Lu/^{177}Hf$=0.015 for the average continental crust, while a ratio of 0.022 (Amelin et al., 1999) is used for two mafic samples (J1625, J1759). Initial $^{176}Hf/^{177}Hf$ and epsilon Hf for all analysed zircon domains were calculated using the respective interpreted crystallization age of each sample. The values of average ε_{Hf} (t) and $^{176}Hf/^{177}Hf_{(i)}$ for each sample are reported as mean ±S.D.

4. Results

All U-Pb dating data and Hf-O isotopic results are presented in supplementary file A and B respectively. In the following text, the (meta-)igneous samples from the Orvin-Wohlthat Mountains are ordered from old to young and the last one is a paragneiss sample.

4.1 U-Pb zircon geochronology and Hf-O isotopic composition of samples from the Orvin-Wohlthat Mountains

J1625 Mafic gneiss (Location coordinates: -71.859678; 9.905846)

Zircon grains in this sample are subhedral to anhedral, rounded, stubby or irregular, clear to light brown, 100–150 μm in size with aspect ratios of up to 3 (Fig. 3). CL images show frequent core – mantle structures reflected by a medium-CL core with oscillatory or weak sector zoning and a CL-dark mantle. Besides, a few stubby to slightly elongated zircons appear entirely CL-dark and structureless, with U contents up to 20000 ppm. Thirty-eight analyses were conducted on 34 grains, targeting all zircon domain-types. Zoned cores were analysed on 23 grains, most with typical Th/U ratios of 0.30–0.60. The 9 oldest analyses form an age group with a concordia age of 1152 ± 7 Ma (MSWD = 1.4), which is interpreted as the crystallization age of the sample. The remaining 14 analyses are discordant possibly due to recent and ancient Pb-loss. Fifteen analyses on rims and structureless domains commonly have high to very high U concentrations (1500–20000 ppm) with Th/U ratios of 0.07–0.30, typical of metamorphic zircons. A few of them (e.g. 8.1, 9.1, 28.1, 29.1) with high U contents and low Th/U ratios (0.07–0.28) are concordant at ca. 1083 Ma. This age group documents the Grenville-age metamorphism in this area. Seven analyses on high-U zircon areas and rims have $^{206}Pb/^{238}U$ ages ranging from 460 to 540 Ma (Fig. 4a), representing a later early Paleozoic tectono-metamorphic overprint.

Lu-Hf and O isotope analyses were conducted on thirteen Grenville-age igneous grains. Except for one outlier with a significantly high ε_{Hf} (t) value (+15.3), which could represent accidental ablation of a Pan-African aged domain at depth, the rest show ε_{Hf} (t) values ranging from +2.6 to +7.9 (Fig. 5a) with an average of +4.8 ± 1.8 ($^{176}Hf/^{177}Hf_{(i)}$ = 0.28218 ± 0.00005), corresponding to a two-stage model age of 2.06–1.69 Ga. Their $\delta^{18}O$ values range from 4.5 to 6.6 ‰ with an average of 5.5 ± 0.6 ‰ (Fig. 6a).

J1772 Migmatitic biotite gneiss (-71.889882; 8.835805)

Zircon grains are mostly euhedral to subhedral, stubby to long prismatic, clear to light brown with abundant fractures, 50–300 μm in length with aspect ratios up to 5. In CL images, most zircons exhibit core–rim structures, characterized by oscillatory zoning in the cores and thin, weakly or strongly luminescent rims. However, the oscillatory zones in some cores have been thickened, blurred, and even entirely homogenized due to Grenville-aged and/or Pan-African alteration. Sixteen core analyses with varied CL characteristics show U abundances of 170–1500 ppm and Th abundances of 60–350 ppm, with Th/U ratios of 0.06–0.82. One grain (16.1) gives an age of ca. 1800 Ma and one grain (7.1) is excluded because it is strongly reversely discordant. The remaining 14 analyses define a discordia line with an upper intercept at ca. 1140 Ma and a lower intercept at ca. 510 Ma (Fig. 4b). The former is interpreted as an approximate crystallization age of an igneous protolith, whereas the latter represents the timing of Pan-African metamorphism.

Lu-Hf isotopic analyses were completed on fourteen grains with different degrees of lead loss, but $^{176}Hf/^{177}Hf$ and Lu/Hf ratios are uncorrelated with Th, U contents and age, indicating the resistance of Hf isotopic composition during subsequent metamorphism. Except 3 analyses which yield significantly positive $\varepsilon_{Hf}(t)$ values between +5.3 and +9.6 (Fig. 5a), the remaining 11 analyses define a uniform isotopic composition with $\varepsilon_{Hf}(t)$ values from +0.9 to +3.6 ($^{176}Hf/^{177}Hf_{(i)} = 0.28217 \pm 0.00003$) and model ages of 1.89–1.72 Ga.

J1807 Granitic orthogneiss (-71.784806, 10.234231)

Zircons are subhedral and elongated, composed of a relatively bright core with oscillatory zoning and structureless rims significantly dark in CL images (Fig. 3). Twenty-eight analyses were obtained on 22 rims and 6 cores. The core and rim domains show distinct difference in U concentration and Th/U ratio; the U content of the cores is generally below 500 ppm and Th/U ratio ranges from 0.19–0.36, while the rims have U contents of several thousand ppm and Th/U ratio between 0.01–0.13. ^{208}Pb-corrected isotopic ratios were used to calculate for rim areas while no correction was necessary for the core analyses. Six core analyses show significant scatter due to Pb-loss. The 3 most concordant cores provide a concordia age of 1130 $\pm$11 Ma (MSWD = 1.03), which is interpreted to represent the crystallization age of the igneous protolith. The rim analyses give two age populations, 20 of which define a well-constrained concordia age of 526 ± 3 Ma (MSWD = 1.17) while the other 2 are (nearly) concordant at ca. 580 Ma (Fig. 4d). They are interpreted to record the timing of multiple high-grade metamorphic overprint.

J1788 Granitic orthogneiss (-71.457797; 11.544662)

Zircons in this sample are euhedral to subhedral, slightly rounded, up to 150 μm in length with aspect ratios of 2 to 3. In CL images, the main portions of the zircons appear oscillatory zoned (Fig. 3) and a few have metamict cores. Many zircons have thin CL-bright rims, though too thin to be analysed. Twenty analyses were performed on oscillatory- and band-zoned domains, which are characterized by relatively uniform Th/U ratios of 0.3–0.5 with Th = 50–310 ppm and U = 180–800 ppm. Twelve analyses yield a concordia age of 1128 ± 5 Ma (MSWD=1.4), interpreted as the crystallization age of the igneous protolith. The remaining 9 discordant analyses are affected by recent Pb-loss (Fig. 4c).

The ε_{Hf} (t) values range from 5.5 to 6.7 (Fig. 5a) with an average of +6.0 ± 0.4 ($^{176}Hf/^{177}Hf_{(i)}$ = 0.28224 ± 0.00001), corresponding to a two-stage model age of 1.59–1.52 Ga. The $\delta^{18}O$ values range from 6.3 to 7.4 ‰ with an average of 7.0 ± 0.3 ‰ (Fig. 6b).

J1793 Tonalitic gneiss (-71.916417; 11.559102)

This sample contains zircon grains that are euhedral to subhedral, transparent, bright and clear, up to 200 μm long with aspect ratios of 2–3. In CL images, zircons show bright to medium oscillatory zoned cores with or without dark unzoned rims which are mostly too thin to be analysed (Fig. 3). Thirty analyses were carried out on 28 cores and 2 rims. The zircons contain very little common Pb. The Th/U ratios of the cores range between 0.29–0.68, with Th=60–250 ppm and U=150–980 ppm. A concordia age of 1118 ± 3 Ma (MSWD = 1.3) is calculated from 17 core analyses, whilst a few other core analyses showed slight signs of Pb-loss and were excluded from the age calculation (Fig. 4e). One of the analysed rims is discordant but has a similar Mesoproterozoic age as the cores (Th/U = 0.26), and may be of metamorphic origin. The other rim analysis (Th/U = 0.01) plots on the concordia curve at ca. 566 Ma. The core analyses are interpreted as the crystallization age of the igneous protolith, whereas the one younger rim analysis represents metamorphic overprint.

Twelve isotopic analyses on concordant igneous domains define a population with a homogeneous Hf-O isotopic composition. The ε_{Hf} (t) values range from +6.3 to +7.9 (Fig. 5a) with an average of +7.1 ± 0.5 ($^{176}Hf/^{177}Hf_{(i)}$ = 0.28228 ± 0.00001), corresponding to two-stage model ages of 1.53–1.43 Ga. Their $\delta^{18}O$ values range from 6.1–6.9 ‰ with an average of 6.5 ± 0.2 ‰ (Fig. 6c).

J1693 Granitic orthogneiss (-71.846046; 9.885719)

Zircon grains are euhedral to subhedral, equant to elongated with aspect ratios of 2–3, clear to light brown and 150–300 μm long. In CL images, many zircons show oscillatory zoned cores that are surrounded by rims (Fig. 3). A few individual zircons are completely CL-dark and structureless. The zircons were analysed in 27 spots, including 20 oscillatory zoned cores and in 7 CL-dark structureless domains. The core analyses show a significant scatter and are in part discordant. The 8 most concordant analyses yield a concordia age of 1108 ± 10 Ma (MSWD = 1.3). Of the 7 rim analyses, two are discordant and the remaining 5 analyses provide a concordia age of 500 ± 4 Ma (MSWD = 0.87) (Fig. 4f). The age of ca. 1108 Ma is the best estimate for the crystallization age of the igneous protolith, whilst the rim analyses of ca. 500 Ma are interpreted as the timing of a metamorphic overprint.

Fourteen Lu-Hf isotopic analyses have been conducted on concordant or nearly concordant igneous domains. Except one with inclusions, the remaining 13 analyses range in ε_{Hf} (t) from 1.1 to 5.5 (Fig. 5a) with an average of +2.7 ± 1.2 ($^{176}Hf/^{177}Hf_{(i)}$ = 0.28216 ± 0.00004), corresponding to two-stage model ages of 1.85–1.58 Ga. Oxygen isotope analyses yield $\delta^{18}O$ values ranging from 5.7 to 8.0 (mean= 7.1 ± 0.7 ‰, Fig. 6d).

J1738 Garnet-biotite orthogneiss (-71.976795l; 9.692059)

Zircons are subhedral to anhedral mostly with rounded terminations, clear to bright brown and 150–300 μm in length with aspect ratios up to 3. They are generally medium to dark in CL, with weak oscillatory zoning overprinted by thin dark rims (Fig. 3). Twenty-two analyses were performed on 21 oscillatory zoned cores and one rim. The Th/U ratio of the cores range between 0.04–0.54 with Th=25–180 ppm and U=90–1660 ppm, and the rim has a Th/U ratio of 0.01. Five of the oscillatory zoned cores give a concordia age of 1107 ± 8 Ma (MSWD = 1.3), whilst the other analyses are discordant due to recent and Pan-African Pb-loss (Fig. 4g). The age of 1107 ± 8 Ma is interpreted to represent the igneous crystallization age of the granite protolith. Metamorphic overprint is evident from one rim analysis at ca. 560 Ma.

J1734 Garnet-biotite orthogneiss (-71.972900; 9.765919)

Zircon grains are subhedral to anhedral, with rounded terminations, light brown to clear, 150–450 μm long with aspect ratios generally between 2 and 3 but sometimes up to 7 (Fig. 3). Although many of the grains are dark in CL, oscillatory zoning can be observed. Many of the grains have a thin dark rim, but in most cases, they are too thin to be analysed. Twenty-three zircon grains were analysed, of which 22 are cores and one rim. The core analyses have Th/U ratios ranging from 0.03 to 0.87, with Th=30–290 ppm and U=340–2200 ppm, and the rim analysis has a Th/U ratio of 0.01. Twelve of the oscillatory zoned cores give a concordia age of 1102 ± 4 Ma (MSWD = 1.12), whilst the others show signs of recent Pb-loss. The only one rim analysis is nearly concordant and gives an age of ca. 540 Ma (Fig. 4h). The concordia age of 1102 ± 4 Ma is interpreted to represent the crystallization age of the igneous protolith with the younger rim analysis attributed to later metamorphism.

The $\varepsilon_{Hf}(t)$ values from concordant or nearly concordant magmatic domains are between -0.2 – +2.4 (Fig. 5a) with an average of +1.2 ± 0.7 ($^{176}Hf/^{177}Hf_{(i)}$ = 0.28212 ± 0.00002), corresponding to two-stage model ages of 1.92–1.76 Ga. Fifteen $\delta^{18}O$ values range from 7.8 to

9.5 ‰ with an average of 8.5 ± 0.5 ‰ (Fig. 6h).

J1792 Granitic orthogneiss (-71.772930; 11.692213)

Zircon grains are mostly subhedral to anhedral with elongate or equant morphologies, yellowish and small (30–120 μm long) with aspect ratios of 1.5–2. In CL images, most of them are characterized by weakly-luminescent oscillatory zoning. A few grains show resorption and a thin, moderately-strongly luminescent overgrowth. Fifteen analyses were performed on zircon cores. These domains have relatively low U (150–750 ppm) and Th (70–340 ppm) contents, with Th/U ratios of 0.12–0.78. Four analyses have been excluded: two with high common lead (3.1, 8.1) and two that are significantly reversely discordant (10.1, 13.1). Ten of the remaining 11 analyses define a concordia age of 1100 ± 5 Ma (MSWD = 1.3) (Fig. 4i).

Lu-Hf isotope analyses were conducted on twelve igneous zircons. Except one Hf analysis with an unusually high ε_{Hf} (t) value at +11.7, the others range in ε_{Hf} (t) from +6.5 to +8.4 (Fig. 5a) with an average of +7.2 ± 0.9 (^{176}Hf/^{177}Hf$_{(i)}$ = 0.28230 ± 0.00003), corresponding to two-stage model ages of 1.53–1.42 Ga. The δ^{18}O values range from 5.7 ‰ to 7.2 ‰ with an average of 6.1 ± 0.4 ‰ (Fig. 6e).

J1690 Charnockite (-71.922297; 8.768715)

Zircon grains are subhedral, elongated, clear, 200–600 μm long with aspect ratios up to 4. In CL images, zircons show oscillatory zoning of inclusion-rich cores that are surrounded by mostly structureless dark rims (Fig. 3). Twenty-seven cores and 5 rims were analysed. Twenty-seven core analyses, including one potential inherited zircon at ca. 1200 Ma, show a scatter due to Pb-loss in some analyses. The 8 most concordant cores provide a concordia age of 1097 ± 14 Ma (MSWD = 1.9). Five rim analyses are all slightly discordant and have a weighted mean ^{206}Pb/^{238}U age of ca. 560 Ma (Fig. 4j). The former age is interpreted as the crystallization age of the igneous protolith, whilst the latter is interpreted to represent the age of charnockitisation.

Lu-Hf isotopic analyses were conducted on 13 igneous domains. Two analyses with higher ε_{Hf} (t) values possibly due to a mixture of core and rim domains have been excluded from the data-averages. The remaining 11 ε_{Hf} (t) values vary from +4.1 to +6.7 (Fig. 5a) with an average of +5.0 ±0.8 ($^{176}Hf/^{177}Hf_{(i)}$ = 0.28223 ±0.00002), corresponding to two-stage model ages of 1.67–1.50 Ga. O isotopic analyses have a $\delta^{18}O$ value from 5.3‰ to 7.1‰ with an average value of 6.6 ±0.5 ‰ (Fig. 6f).

J1672 Granitic orthogneiss (-71.778109; 10.553229)

Zircons are subhedral to anhedral with rounded terminations, up to 300 μm long, with aspect ratios of 2–3. Many of the zircons show oscillatory zoning with thin, dark, structureless rims that were mostly too thin to be analysed (Fig. 3). Twenty-six zircon domains were analysed, including 21 zoned grains and 5 rims. The rims have a Th/U ratio ranging from 0.005 to 0.26, and the cores have Th/U ranging from 0.19 to 0.65 with Th=35–510 ppm and U=100–800 ppm. Nineteen analyses of oscillatory zoned cores give a concordia age of 1090 ±4 Ma (MSWD = 0.95). The other 2 core analyses show Pb-loss, and/or have high analytical error. Three rim analyses yield a concordia age at ca. 560 Ma (Fig. 4k). The age of ca. 1090 Ma is interpreted as the crystallization age of the igneous protolith and the rim analyses of ca. 560 Ma are regarded as the time of metamorphic overprint.

Lu-Hf and O isotope analyses were conducted on fifteen concordant igneous domains. One Hf analysis yielded an aberrantly high ε_{Hf} (t) value at +11.0, whilst the other values range from +6.3 to +8.4 (Fig. 5a) with an average of +7.4 ±0.6 ($^{176}Hf/^{177}Hf_{(i)}$ = 0.28230 ±0.00002), corresponding to two-stage model ages of 1.51–1.38 Ga. $\delta^{18}O$ values range from 6.7 to 7.9 ‰ with an average of 7.1 ±0.3 ‰ (Fig. 6g).

J1759 Amphibolite (-71.722712; 10.629123)

Zircon grains are stubby to short prismatic, clear to light brown, with lengths of 50–300 μm and aspect ratios of 1.5–3. Most zircons display core-rim structures. The former are CL-dark and either show no zoning, sector zoning or oscillatory zoning and the rims are CL-bright and structureless. A few grains are distinctly highly luminescent with dark thin rims. Eleven grains were analysed, 9 of which are from the low-luminescent domains with high U concentrations (570–1640 ppm) and Th/U ratios (0.14–0.46). Most analyses are discordant and plot on a discordia line, with a poorly-defined upper intercept at 1084 ±68 Ma (MSWD = 0.73, Probability = 0.74) and a lower intercept at ca. 600 Ma (Fig. 4l). The upper intercept at ca. 1084 Ma is interpreted as being close to the crystallisation age of the igneous protolith, whilst the lower intercept is probably related to metamorphic overprint and the time of lead-loss. The remaining two zircon domains with high luminescence (10.1, 11.1) have much lower U-concentrations (250–280 ppm) and higher Th/U ratios of 0.62–0.83. One of them is highly discordant and thus excluded from the calculation. The other one gave an older age of ca. 1.2 Ga, which may represent an inherited domain.

Lu-Hf isotopic analyses have been done on twelve igneous grains with different degrees of lead loss. They display a spread in Hf isotopic composition, with ε_{Hf} (t) values ranging from +5.1 to +12.1 (Fig. 5a, $^{176}Hf/^{177}Hf_{(i)}$ = 0.28224 – 0.28244) and two-stage model ages from 1.79 to 1.17 Ga.

J1851 Granitic augen gneiss (-71.574047; 12.146767)

The sample contains euhedral to subhedral, clear to light brown zircons, 200–400 μm long with aspect ratios up to 5. In CL images, most grains appear bright with oscillatory growth zoning (Fig. 3). Some have minor, dark rims that were too thin to be analysed. Twenty-seven spots were analysed, all from the oscillatory zoned cores. The analyses show a significant scatter due to Pb-loss. Two analyses, including one with a large error (15.1) and the other with high discordance (7.1), are excluded from plotting. The most concordant analyses provide a well-constrained concordia age of 1081 ±5 Ma (MSWD = 1.3, n = 11, Fig. 4m). This age is interpreted as the igneous crystallization age of the igneous protolith.

Fifteen O isotopic analyses on igneous domains have a $\delta^{18}O$ value from 8.3‰ to 9.5‰ with an average value of 8.9 ± 0.4 ‰ (Fig. 6j). The ε_{Hf} (t) values range from +4.5 to +7.1 (Fig. 5a) with an average of +5.8 ± 0.9 ($^{176}Hf/^{177}Hf_{(i)}$ = 0.28226 ± 0.00002), corresponding to two-stage model ages of 1.62–1.46 Ga.

J1710 Garnet-biotite orthogneiss (-72.143052; 10.013868)

Zircon grains are anhedral, stubby to elongate and clear to brownish. Some grains are cracked and many have inclusions. Many zircons have clear core-mantle structures. In CL images, zircons show mostly oscillatory zoned cores with moderate CL response. The cores have CL-dark, structureless rims, often thick enough at their tips to be analysed (Fig. 3). Few zircons are composed of oscillatory zoned core, CL-moderate mantle and dark rim (Fig. 3). Twenty-five spots were analysed on 18 cores, 1 mantle and 6 rims. Most core analyses have Th/U ratios ranging from 0.18 to 0.86, whilst most rim domains have very high U concentrations up to 6600 ppm with typical Th/U ratios below 0.1. Of the 18 core analyses two inherited zircon domains plot on the concordia curve at ca. 1200 Ma, and 6 analyses form a uniform age group with a concordia age of 1079 ± 8 Ma (MSWD = 0.74) (Fig. 4n). Some zircon cores appear to have recrystallized to some extent to have a low Th/U ratio (< 0.2). The core analyses of ca. 1079 Ma are interpreted as the best estimate for the crystallization age of the granitic protolith. A mantle and a rim domain yield ages of ca. 1030 Ma and ca. 1080 Ma respectively, which are regarded as the timing of a subsequent metamorphic event. Furthermore, the 1000–900 Ma and 500 Ma discordant zircons may record evidence of multistage metamorphism in early Tonian and Cambrian times.

Lu-Hf and O isotope analyses were performed on fourteen concordant or nearly concordant grains with Grenville-age igneous ages.The ε_{Hf} (t) values range from -2.8 to +1.1 (Fig. 5a) with an average of -0.4 ± 1.1 ($^{176}Hf/^{177}Hf_{(i)}$ = 0.28209 ± 0.00003), corresponding to two-stage model ages of 2.07–1.82 Ga. Eleven analyses have $\delta^{18}O$ values ranging from 7.7 to

10.0 ‰ with an average of 9.0 ± 0.8 ‰ (Fig. 6i), while three outliers with lower $\delta^{18}O$ values are excluded from average calculation.

DML 40 Garnet-sillimanite-cordierite gneiss (metapelitic paragneiss) (-71.965033, 7.367933)

This is the only meta-sedimentary sample of this study. It is a garnet-sillimanite-cordierite gneiss with melanocratic layers alternating with leucosome layers. Zircon grains are subhedral, short columnar with a maximum length of ca. 200 μm. CL images of most zircons show oscillatory zoned cores surrounded by dark, unzoned rims (Fig. 3). Twenty-three analyses were conducted on core domains, which have high Th/U ratios ranging from 0.16 to 0.89. Seven of them yield a concordant age at 1139 ± 11 Ma (MSWD = 0.78), 3 grains were dated at ca. 1750 Ma, and 6 have Mesoproterozoic (Ectasian) ages of 1320–1200 Ma. Other analyses on cores are discordant because of Pb-loss (Fig. 4o). Fourteen analyses were performed on rim domains. Low Th/U ratios (0.01–0.16) with Th=4–161 ppm and U=344–2193 ppm may indicate a metamorphic origin. The 5 youngest rim analyses form a well-constrained age group with a concordia age of 526 ± 6 Ma (MSWD = 0.81). The other rim analyses are discordant with an age of 850–800 Ma and ca. 610 Ma (Fig. 4o).

The core age spectrum from ca. 1770–1220 Ma represent detrital zircon components from Paleoproterozoic to Ectasian source regions. The youngest concordant detrital ages are ca. 1140 Ma and likely represent the maximum depositional age of the sedimentary protolith, coinciding with the older age spectrum of igneous rocks in this study. The rim age of 526 ± 6 Ma is interpreted to represent crystallization of anatectic melt during cooling from peak temperatures.

4.2 Hf-O isotopic signature of samples from Gjelsvikfjella

Six granitic gneiss samples that had been U-Pb zircon dated previously (Jacobs et al., 2003a, 2008b) were analysed for their Hf-O isotopic compositions (Table 1, Fig. 5c-d and 7). Despite a broad spread in Hf isotopic composition observed in several samples, the two-stage

Hf model ages cluster between 1.75–1.55 Ga with a peak at 1.67 Ga (Fig. 5d), which are distinct from those of the Orvin-Wohlthat Mountains (Fig. 5b). Zircons dominantly have an oxygen isotopic composition in the range of mantle values (5.3 ± 0.6, 2σ, Valley et al., 1998) but a few (e.g. sample 1701-2) display low $\delta^{18}O$ values (Fig. 7a).

Table 1 Zircon Hf-O isotopic data of samples from Gjelsvikfjella

Sample	Rock types	Igneous age (Ma)	$^{176}Hf/^{177}Hf_{(t)}$	ε_{Hf} (t)	ε_{Hf} (t) ± S.D.	$\delta^{18}O$ (‰)
1701-2	Migmatitic gneiss	1142 ± 10	0.28219–0.28230	+3.6 – +6.8	5.3 ± 1.5	2.9–4.3
1812-5	Migmatitic augen gneiss	1137 ± 14	0.28217–0.28224	+3.8 – +6.4	4.9 ± 0.7	4.5–6.1
1512-1	Augen gneiss	1123 ± 21	0.28216–0.28223	+3.1 – +5.7	4.3 ± 0.8	5.0–6.5
2712-4	Migmatitic gneiss	1115 ± 12	0.28207–0.28231	-0.1 – +8.3	3.7 ± 2.2	4.3–7.6
2412-4	Migmatitic augen gneiss	1096 ± 8	0.28219–0.28228	+3.4 – +6.6	4.8 ± 0.9	4.6–5.9
3012-1	Mylonitic felsic gneiss	1098 ± 25	0.28206–0.28221	-1.1 – +4.4	2.0 ± 1.1	4.2–5.6

4.3 Summary of zircon geochronological and Hf-O isotopic data

The U-Pb geochronological results of the 15 newly dated samples are summarized in Fig. 8. The igneous ages show a protracted and almost continuous magmatism from 1160 Ma to 1070 Ma, with an age concentration at ca. 1110–1090 Ma. Some samples also show Mesoproterozoic metamorphic ages, which are recorded by single grains or rim overgrowths, characterized by dark CL and low Th/U at ca. 1080–1030 Ma. Most samples also exhibit a metamorphic overprinting history between 600 and 500 Ma. Zircon inheritance is rare, with ca. 1200 Ma ages recorded by a few samples and ca. 1700 Ma by one sample. No early Paleoproterozoic or Archaean inherited zircons were found. Detrital zircons from the only meta-sedimentary sample (DML 40) yield U-Pb ages clustering around 1750 Ma, 1320–1200 Ma and 1140 Ma, overprinted by Cambrian (ca. 530 Ma) metamorphism. Most samples from the Orvin-Wohlthat Mountains have $\delta^{18}O$ values that are similar to, or slightly higher than, mantle values and have strongly positive ε_{Hf} (t), while a few samples (e.g. J1710, J1734; Fig. 5) with a mineralogical affinity to S-type granites (garnet-bearing) display distinctly higher $\delta^{18}O$ and lower ε_{Hf} (t) values. Five of six samples from Gjelsvikfjella have mantle-like O and suprachondritic Hf-isotopic compositions, whereas one sample has a lower $\delta^{18}O$ value (2.9–

4.3 ‰) than mantle value.

5. Discussion

5.1 Mesoproterozoic crustal growth and reworking in cDML

Magmas generated in subduction zones commonly contain components sourced from a number of different reservoirs, such as the subducted oceanic slab and sediments, the mantle wedge, and overlying crustal material of different ages and provenance (Pearce et al., 1999; Elburg et al., 2002; Bindeman et al., 2005). Combined zircon Hf-O isotopic investigations have the potential to constrain variable contributions of juvenile (directly mantle-derived) versus pre-existing continental components in source rocks and parent melts (e.g. Lancaster et al., 2011; Roberts and Spencer, 2015; Payne et al., 2016). Such data allow us to track the magmatic source characteristics of the Grenville-age samples collected from cDML and thus provide important insights into the history of crustal growth and recycling during orogenesis.

5.1.1 Orvin-Wohlthat Mountains

Meta-igneous samples from the Orvin-Wohlthat Mountains predominantly give igneous crystallization ages of 1110–1090 Ma. They show a broad variation in zircon Hf and O isotopic compositions (Fig. 9a), implying the involvement of multiple mantle- and crust-derived components in the source. Most samples show moderately elevated $\delta^{18}O$ values between 6.4 and 7.1 ‰ (Fig. 6, 9a), a composition typical of I-type arc rocks (Eiler, 2001; Kemp et al., 2007). A large proportion of zircons from these samples (red in Fig. 5a) display suprachrondritic ε_{Hf} (t) values, with the averages lying slightly below the composition of the arc mantle array presented by Dhuime et al. (2011) and corresponding to Mesoproterozoic model ages (Fig. 5b). This indicates that the parental magmas are rather juvenile with limited contribution from ancient continental components, either in the melt source region or by crustal contamination. The absence of any significantly older inherited zircons provides further evidence for minor to negligible interaction of these magmas with old continental crust. Sample J1851 displays an average ε_{Hf} (t) value of +5 in association with elevated $\delta^{18}O$ values (8–10 ‰), suggesting a derivation from mixing of juvenile, mantle-derived magma with young supracrustal components, either altered volcanic crust or sedimentary rock.

The addition of ancient crustal material to arc magmas in this region is also revealed by a group of samples with enriched Hf isotope compositions (Fig. 5a, b). Two samples (J1710, J1734) have distinctively elevated $\delta^{18}O$ values at 8.5–9.0‰ (Fig. 6h, i) associated with unradiogenic ε_{Hf} (t) and Paleoproterozoic model ages (Fig. 5b). The Hf-O isotopic signatures combined with the presence of garnets and whole-rock elemental data comparable to S-type granite (e.g. high A/CNK>1.0, unpublished data) indicate a significant contribution from ancient sedimentary supracrustal material. The addition of the sedimentary material could be achieved by source contamination, i.e. the inclusion of subducted sediments overlying the oceanic crust, or by assimilation and re-melting of sedimentary components from overlying arc crust. The latter mechanism is preferred here, as previous studies show that in arc magmas, the contribution of heavy $\delta^{18}O$ from the subducted material can be very limited (e.g. Vroon et al., 2001). Whatever explanation, the Hf model ages ranging from 2.1 to 1.8 Ga suggest that the sediments could possibly have a Paleoproterozoic or older age, which then were most likely derived from the Proto-Kalahari Craton. The other two samples (J1693 and J1772) with a more depleted but heterogeneous Hf isotopic composition may be derived from a mixing of old sedimentary material and juvenile magmas.

The oldest sample in this study (mafic gneiss J1625, 1152 ± 7 Ma), which has a relatively homogeneous mantle-like $\delta^{18}O$ value (Fig. 6a), exhibits, however, a spread in Hf isotopic composition (ε_{Hf} (t)= 2.6–7.9, Fig. 5a). This indicates that this sample was most likely derived from juvenile mantle-derived magmas mixed with recycled older continental crust. The post-1110 Ma zircons with a moderate $\delta^{18}O$ value commonly have a more juvenile Hf isotopic composition than the older ones (Fig. 5a), suggesting an overall increasing input of mantle-derived magmas from 1150 Ma to 1090 Ma.

5.1.2 Gjelsvikfjella

In contrast to the Orvin-Wohlthat Mountains samples, which show significant inter-sample variation in Hf-O isotopic composition, the samples from Gjelsvikfjella have broadly similar isotopic signatures (Fig. 9a). The mantle-like $\delta^{18}O$ value (4.5–6.0‰) exhibited by most zircons shows little influence of supracrustal components, such as sediments, in the source. Most zircons display suprachondritic Hf isotopic characteristics, although with lower ε_{Hf} (t) values than zircons crystallized from juvenile magmas in the Orvin-Wohlthat Mountains, and yield a peak of model ages at 1.7–1.6 Ga (Fig. 5c, d). Assuming these rocks were dominantly crust-derived, the model age represents either the real age when the crust was extracted from the depleted mantle, or an average age of the various components contributing to the magma. These crustal component(s) must have resided for an extended period at depth since separation from the mantle reservoir, in order to avoid hydrothermal alteration that would have driven their oxygen isotopic signature to higher values than those measured. The spread of ε_{Hf} (t) values and model ages (2.0–1.4 Ga) may reflect a heterogeneous source composition composed of both older Paleoproterozoic and Mesoproterozoic crustal components. Alternatively, a source consisting of both older components and juvenile additions could also explain the Hf-O isotopic signature of these samples. In this scenario, the reworked crustal components must be older than the calculated model age, and involvement of Paleoproterozoic and/or Archean crust is possible. The mixing of juvenile magmas and older components is indicated by sample 2712-4, which displays both mantle-like and moderate high $\delta^{18}O$ and variable ε_{Hf} (t) values (Fig. 5c, 6d). Therefore, it is evident that ancient crust was involved in the formation of the Grenville-age samples in Gjelsvikfjella.

Some zircons (e.g. all zircons from sample 1701-2) yield an average $\delta^{18}O$ value below the 2σ lower uncertainty of the mantle reference value (< 4.7 ‰, Valley et al., 1998), associated with depleted Hf isotopic compositions. Zircons with low $\delta^{18}O$ values are commonly interpreted to have been crystallized from originally ^{18}O-poor magmas (Zheng et al., 2004; Hiess et al., 2011; Rehman et al., 2018), although post-magmatic hydrothermal alteration has also been proposed to interpret low $\delta^{18}O$ values in metamict zircons (Iizuka et al., 2013). The low-$\delta^{18}O$ zircons in this study most likely inherited the oxygen isotopic compositions from parental magmas, which had probably obtained light oxygen isotopes by fluid-rock interaction at a high temperature in subduction zone, and/or involving isotopically light meteoric water.

5.1.3 Summary of Grenville-age crustal evolution in cDML

In summary, the zircon Hf-O isotopic data from cDML show apparently contradictory results (Fig. 9a). On the one hand, the paucity of ancient inherited zircons, radiogenic Hf isotopic compositions shown by supra-chondritic $\varepsilon_{Hf}(t)$ values and Mesoproterozoic model ages of most orthogneiss samples from the Orvin-Wohlthat Mountains are compelling evidence that they are of predominantly juvenile character. Conversely, re-melting of sedimentary rocks derived from the erosion of older basement, and of the basement at the edge of the Proto-Kalahari Craton itself is indicated by (meta)granitic rocks from the Orvin-Wohlthat Mountains which are characterized by high $\delta^{18}O$ values (8.0–10.0 ‰) and evolved Hf isotopic signatures, and from Gjelsvikfjella samples with Paleoproterozoic Hf model ages and mantle-like oxygen isotopic compositions.

The data suggest therefore that both processes, juvenile addition and crustal recycling, were operative in the generation of the granitoids of cDML during Grenville-age orogenesis.

5.2 Grenville-age continental arc magmatism in the Maud Belt

Whether the arc magmatism of the Maud Belt developed on oceanic or continental substrates remains controversial; our data show that, in cDML, a combination of juvenile and reworked crust was instrumental in producing the voluminous granitoids. Although the Maud Belt is now adjacent to the Archean Grunehogna Craton where basement outcrops were dated at ~ 3.1 Ga (Barton et al., 1987; Marschall et al., 2010), there is only sparse evidence of incorporation of the Archean components in its Grenville-age magmas. Instead, previous work reported relatively juvenile Nd isotopic composition in most sections of the Maud Belt with dominant early Mesoproterozoic/late Paleoproterozoic model ages (e.g. Arndt et al., 1991; Jacobs et al., 1998; Wareham et al., 1998; Grantham et al., 2011). The Maud Belt was thus interpreted by some researchers as a number of exotic island arcs that accreted onto the craton margin (e.g. Bauer et al., 2003a; Grosch et al., 2007; Grantham et al., 2011). However, our new zircon Hf-O isotopic data show that the amount of older crust (most likely Paleoproterozoic in age) that was incorporated into the source of Grenville-age magmas is greater than previously recognized (Section 5.1). Moreover, the juvenile input to arc magmas, as recorded in the Orvin-Wohlthat Mountains samples, does not equate with an absence of continental crust overlying the subduction zone. In Andean-type orogens, the overlying continental crust makes a variable contribution to arc magmas during the evolution of the arc system. Juvenile magmas with minor to negligible contamination from older crust are commonly emplaced when subduction retreat and the ocean-ward migration of the arc cause crustal thinning (Cawood et al., 2009; Boekhout et al., 2015). For example, the southern Central Andes experienced a progressive input of mantle-derived melts over several tens of million years with little recycling of pre-existing crustal material (Jones et al., 2015).

Zircon Hf-O isotopic data in this study provide crucial information on the crustal composition along the eastern margin of the Proto-Kalahari Craton, which is important for the better understanding of the nature and geodynamics of the Maud Belt. We speculate that Paleoproterozoic components existed or still exist in this region based on following lines of evidence in addition to our new data. Firstly, detrital zircons from the Mesoproterozoic

Ritscherflya Supergroup, which were most likely derived from the Maud Belt, exhibit the growth of ca. 1130 Ma igneous zircons on 1.9–1.7 Ga cores, indicating the development of Grenville-age magmatism on Paleoproterozoic basement (Marschall et al., 2013). Secondly, Paleoproterozoic inherited zircons, although rare, have been discovered in various parts of the Maud Belt (e.g. Baba et al., 2015; Ksienzyk and Jacobs, 2015 and this study) and hints of such sources are even present in the adjacent Natal-aged crust (e.g. Arndt et al, 1991; Mendonidis and Thomas, 2019). Moreover, 1.3–1.2 Ga detrital zircons (sample DML 40 in this study and Baba et al., 2015) and a few 1.2 Ga inherited zircons may imply a more complicated crustal composition in this region with a Mesoproterozoic (Ectasian) component, although the origin of these detrital zircons is enigmatic since much of the southern Kalahari and Laurentia margins preserve similar geochronological records of this period. In view of the above, it is therefore not tenable to consider the Maud Belt as a single island arc edifice. It was more likely built upon pre-existing crust along the margin of the Proto-Kalahari Craton.

The Grenville-age magmatism in the Maud Belt shows significant spatial variation, with radiogenic isotopic compositions becoming increasingly juvenile towards the east (Fig. 9b). Samples from the H.U. Svedrupfjella (closest to the Grunehogna Craton) are characterized by negative ε_{Nd} (t) values associated with Paleoproterozoic to Archean model ages (Wareham et al., 1998; Grosch et al., 2007), suggesting a large degree of reworking of older basement crust underlying the Proto-Kalahari Craton (Fig. 2). In Gjelsvikfjella, Hf model ages of zircon grains with mantle-like O isotopic composition yield a peak at late Paleoproterozoic times, which indicates a significant contribution from pre-existing crustal material. In the Orvin-Wohlthat Mountains, east of the Ulvetanna Lineament, the samples with addition of old crustal material are mainly exposed in the western part (W of 10°E), while the Grenville-age component in the eastern part is mainly composed of 1120–1080 Ma juvenile rocks (Fig. 9b). This spatial isotopic trend is consistent with the characteristics of continental-arc magmatism, which commonly incorporates more isotopically evolved continental crust landward (Chapman et al., 2017). The Orvin-Wohlthat Mountains most probably represent the accretionary terrane overlying the inboard subduction zone beneath the Proto-Kalahari Craton, with a transition in source composition of Grenville-age rocks from ancient craton-derived to younger oceanic-crust related material towards the east. In this scenario, the Ulvetanna Lineament (Fig. 2) may represent the boundary between an accretionary complex and the cryptic edge of the continental crust of the Proto-Kalahari Craton.

A group of ~1100 Ma igneous ages in our dataset from cDML indicates a significant magmatic episode between the emplacement of early arc magmas and late-stage tectono-thermal events. In adjacent areas, magmatic activity at this time produced the Borgmassivet mafic/ultramafic sills intruding the Ritscherflya Supergroup in the Grunehogna Craton, which were interpreted as subduction-related magmatism in some studies (Grosch et al., 2015; Hokada et al., 2019). An opposing opinion considers that the mafic intrusions form part of the Umkondo Large Igneous Province (LIP) emplaced in the interior of the Proto-Kalahari Craton (e.g. Moabi et al., 2017). From a global perspective, the Umkondo magmatism is coeval with several other LIPs in Laurentia including the Coats Land block, Amazonia, Congo and in the cratons of India (e.g. Davis and Green, 1997; Ernst et al, 2013; de Kock et al., 2014; Teixeira et al., 2015). These large-scale intraplate magmatic events could be a consequence of anomalously high mantle heat flow in the Mesoproterozoic, which might have been independent of the supercontinent cycle (Hanson et al., 2004). The relationship between the synchronous Umkondo LIP and the subduction-related magmatism along the margin of Kalahari remains ambiguous (e.g. Hanson et al., 1998, 2004; Hokada et al., 2019). In the Orvin-Wohlthat Mountains, apparently more juvenile Hf isotopic composition of post-1110 Ma rocks compared to the older orthogneisses argues for a transition in the tectonic setting (Fig. 5a), most likely from an advancing to a retreating accretionary orogenic setting, resulting in the generation of voluminous juvenile magmas. Subsequent granitic magmatism and high-grade metamorphism at 1090–1030 Ma may have taken place under convergence in an overall advancing accretionary tectonic setting. The tectonic switch could be partly related to the changes in mantle convection and global plate reorganisation during eruption and cooling down of plume activities in the Umkondo LIP magmatism.

Grenville-age geochronological records are also preserved in the Nampula Complex in NE Mozambique, lying to the north of the Maud Belt in Gondwana (Fig. 1b). Grenville-age magmatic activity in the Nampula Complex has been well constrained at 1150–1030 Ma (Bingen et al. 2009; Macey et al., 2010; Thomas et al., 2010). The age is comparable to the Maud Belt but distinctly older than other Mesoproterozoic crust to the north (i.e. 1060–950 Ma Marrupa and Unango complexes, Bingen et al., 2009). It is thus envisaged that the Nampula Complex cannot be correlated with these complexes in the north but most likely has a tectonic affinity with the Maud Belt and could possibly be restored to a position along the margin of Proto-Kalahari (Bingen et al., 2009). This is supported by the similarity in Hf isotopic characteristics between these two regions. Thomas et al. (2010) showed that 1.1–1.0 Ga detrital zircons derived from the Nampula Complex yield both juvenile (ε_{Hf} (t) = 5–9) and evolved Hf isotopic compositions with model ages ranging from Mesoproterozoic to Archean times, comparable to the isotopic signature of samples from the Orvin-Wohlthat Mountains in this study. Therefore, the Maud Belt very likely extended northwards into NE Mozambique, constituting a composite Andean-type magmatic arc along the eastern margin of the Proto-Kalahari Craton.

5.3 Implications for the Natal and Maud belts

In Rodinia, the Natal and Maud belts were in relatively close proximity and together formed the western extension of the greater Grenville Orogen. However, although they formed roughly synchronously along the same part of the orogen, their subduction polarity, age and orogen style are distinctly different. Whilst the Natal Belt is best explained as a juvenile arc-continent collision orogen with potential continent-continent collision, the Maud Belt may be better explained as a somewhat younger, outboard accreted arc with a significant (but diminishing eastwards) element of older (Proto-Kalahari) crust, recorded by spatially-controlled differing zircon U-Pb ages and radiogenic isotope signatures of the evolving igneous rocks.

The Natal Belt is characterised by a subduction polarity away from Proto-Kalahari with a passive margin until arc-continental collision commenced at ca. 1150 Ma (Jacobs et al, 1997). Structural, petrological, and paleomagnetic data support the interpretation of continental collision between Proto-Kalahari and Laurentia, with the accreted Natal arcs sandwiched between the two cratonic masses. The changing late shear geometries from dextral in Namaqualand to sinistral in the Natal prompted the hypothesis of the Proto-Kalahari being an indenter into Laurentia (Jacobs et al., 1993, 2003a, 2008). The widespread A-type charnockitic magmatism at 1050–1030 Ma and simultaneous LP-(U)HT metamorphism, followed by isobaric cooling in the Natal sector has been interpreted to take place in a convergent (transpressional) setting (Thomas et al., 1993; Spencer et al., 2015). Recent palaeomagnetic data from the Umkondo large igneous province (LIP) is consistent with the interpretation that Proto-Kalahari had conjoined with Laurentia before 1015 Ma with the Namaqua-Natal Belt oriented towards the Grenville margin of Laurentia (e.g. Swanson-Hysell et al., 2015). The collision of Proto-Kalahari and Laurentia is also supported by the position of the Coats Land Block within Rodinia. The Coats Land Block is interpreted as a part of Laurentia (Loewy et al., 2011) or an exotic terrane accreted to Laurentia (Swanson-Hysell et al., 2015), and may represent a rifted block that was incorporated into Greater Kalahari after collision and dispersal of Rodinia (Gose et al., 1997; Jacobs et al., 2003; Loewy et al., 2011). Grenville-age magmas in the Natal Belt predominantly originated from the reworking of lithospheric substrate of pre-

Rodinian island arcs with negligible addition of ancient crust or mantle-derived magmas (Eglington and Harmer, 1989; Spencer et al., 2015), indicated by Sr, Nd and Hf isotopic compositions of 1175–1030 Ma granitoids with a similar trend to the evolution curve of continental crust (Fig. 5a, c).

In contrast to the Natal Belt, the Maud Belt shows clear evidence for subduction polarity towards Proto-Kalahari within an overall active continental margin setting (e.g. Bisnath et al., 2006; Marschall et al., 2013). However, our new data acquired in this study, together with published data from other parts of the Maud Belt, necessitate a re-appraisal of this simple model. Our new U-Pb geochronological data combined with published geochronological results from the Orvin-Wohlthat Mountains have identified two major periods of Grenville-age magmatism at 1150–1125 and 1110–1090 Ma, comparable to other areas in the Maud Belt (Fig. 10a-e). The age spectra from the Maud Belt is clearly distinguishable from that obtained from the Natal Belt, which has distinct records of pre-1200 Ma island arc magmatism, an age component which is missing in the Maud Belt (Fig. 10f). In the Natal Belt, syn-collisional granitic magmatism and high-grade metamorphism is well constrained between 1050 and 1030 Ma (Thomas et al., 1993; Spencer et al., 2015 and references therein), whereas such ages are very rarely reported in the Maud Belt (Fig. 10f). In further contrast to Natal, samples in the Orvin-Wohlthat Mountains with moderate ^{18}O values define an ε_{Hf} – time trajectory nearly parallel to the evolution trend of the arc mantle in cDML (Fig. 5a), which implies progressive juvenile input to arc magmas. This is commonly documented in active continental margins with continuous subduction processes (e.g. Spencer et al., 2019).

It is thus clear that the Maud and Natal belts cannot be correlated in a simple geodynamic model as originally suggested (e.g. Groenewald et al., 1995). The tectonic contact between the Natal and Maud belts may mark the change from final continental collision to outboard-Proto Kalahari accretionary tectonics at the westernmost end of the greater Grenville

Orogen (Fig. 1 and 11). The Maud Belt probably marks the start of a long-term active continental margin setting along eastern Kalahari, with semi-continuous, west-facing subduction for the subsequent 500 Ma. This tectonic setting may have been activated during subsequent extroversion of Rodinia and closure of the exterior ocean in middle to late Neoproterozoic times. The westward subduction of the Mozambique oceanic slab beneath this margin led to the accretion of TOAST (990–900 Ma) and terminated with the final amalgamation of Gondwana at ca. 550 Ma (e.g. Jacobs and Thomas, 2004).

Summary and conclusions

(1) New SHRIMP zircon U-Pb data provide detailed constraints on the temporal framework of Grenville-age tectono-thermal events in a large part of the Maud Belt. Arc magmatism in Orvin-Wohlthat Mountains occurred from 1160 to 1070 Ma with a culmination at 1110–1090 Ma, followed by high-grade metamorphism at ca. 1080–1030 Ma.

(2) Most zircons from the Orvin-Wohlthat Mountains have positive ε_{Hf} (t) values and Mesoproterozoic model ages, with $\delta^{18}O$ values similar to, or slightly higher than, typical mantle values. This suggests crystallization from juvenile magmas with little recycling of pre-existing continental crust.

(3) In contrast, zircons from Gjelsvikfjella dominantly have mantle-like $\delta^{18}O$ values and more evolved Hf isotopic composition with Paleoproterozoic model ages, indicating more contribution of older crust components from the Proto-Kalahari Craton. The involvement of ancient sediments is additionally reflected by some zircons from the Orvin-Wohlthat Mountains with distinctively lower ε_{Hf} and highly elevated $\delta^{18}O$ values.

(4) The reworking of ancient continental material indicates that the Maud Belt developed on the lithospheric substrate of the Proto-Kalahari Craton margin. A protracted accretionary process associated with westward subduction beneath the craton involving tectonic switching between advancing and retreating subduction processes may best explain the formation of the

cDML part of the Maud Belt during the later stage of Rodinia amalgamation.

(5) A new definition of the younger Maud belt (as distinct from the older Namaqua-Natal belt) can be proposed. Continuous continental arc magmatism in the Maud Belt is tectonically unrelated with the accretion of oceanic island arcs and final continent-continent collision in the Natal Belt. The Natal and Maud belts therefore had independent tectonic evolutions although they both reside along the margin of Proto-Kalahari.

(6) The tectonic contact relationship of the Natal and Maud belts is highly speculative, because it is largely unexposed and/or overprinted by later pan-African tectono-thermal events. The complex and contrasting tectonic evolution of the two belts characterises the lateral western termination of the greater Grenville Orogen. The Maud Belt appears to be the temporal starting point for a protracted accretionary tectonic cycle in the region, which continued from Stenian times into the early Neoproterozoic with the accretion of the TOAST. This accretionary supercycle outlasted almost the entire Neoproterozoic and relates to the extroversion of Rodinia and final formation of Gondwana.

Acknowledgements

This work was financially supported by faculty-specific funds and endowments of the Faculty of Mathematics and Natural Sciences, University of Bergen (No. 812378). C-C. Wang thanks for support from the China Scholarship Council. J. Jacobs thanks for continued field support of the Alfred-Wegener Institute, Bremerhaven, and the Federal Institute for Geosciences and Natural Resources (BGR). We thank M. Whitehouse and H. Jeon for their help in SIMS zircon O isotopic analyses, P. Montero and F. Bea for their help with SHRIMP analyses at the IBERSIMS facility, Granada, and M. Wingate for his help with SHRIMP analyses at Curtin.

The MC-ICPMS lab at UJ was funded by NRF-NEP grant 93208, and is supported by DSI-NRF CIMERA. M. A. Elburg acknowledges NRF IFRR funding (No. 119297). We thank Prof. T. Tsunogae and two anonymous referees for the editorial handing and helpful comments. This is IBERSIMS publication #66 and a contribution to IGCP 648, Supercontinent Cycles & Global Dynamics.

Figure captions

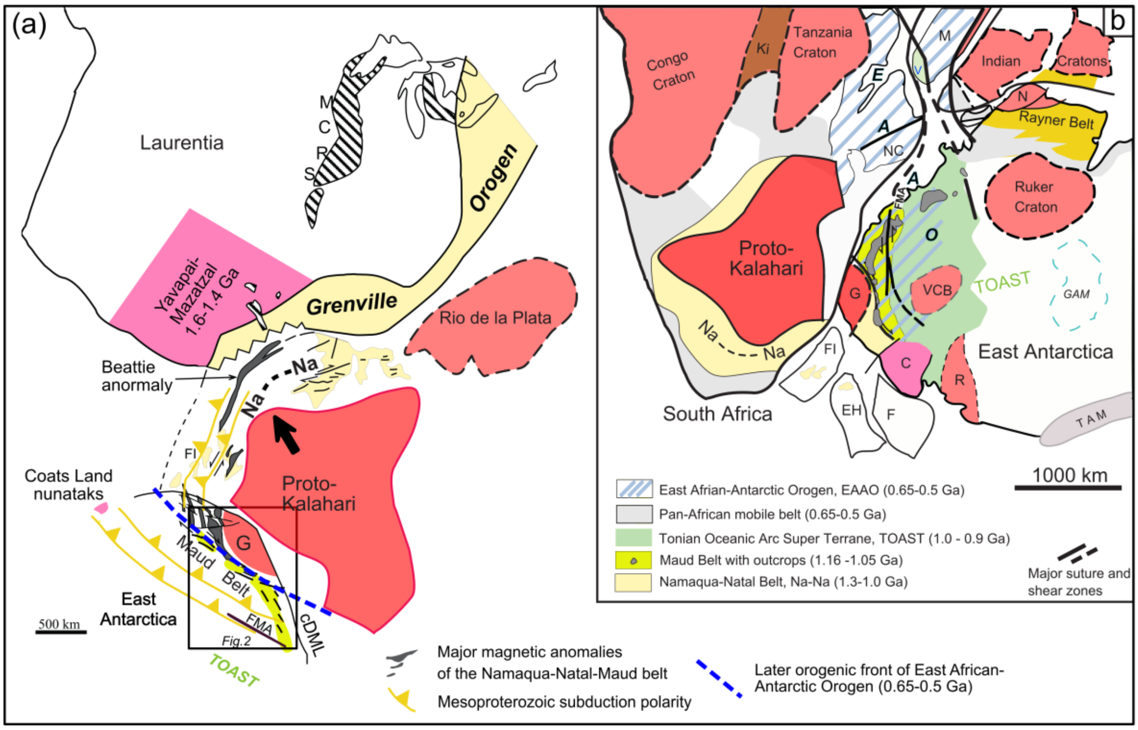

Fig. 1: (a) Reconstruction of the Maud and Namaqua-Natal (Na-Na) belts along the Proto-Kalahari Craton with Laurentia in Rodinia, after Jacobs et al. (2003a). The Proto-Kalahari Craton is interpreted as an indenter into Laurentia to form the Namaqua-Natal Belt at ca. 1050 Ma. The Maud Belt was traditionally regarded as the natural continuation of the Na-Na Belt into East Antarctica (e.g. Groenewald et al., 1995; Bauer et al., 2003), but has later been interpreted as a slightly younger accreted arc terrane (e.g. Mendonidis et al., 2013). Location of Rio de la Plata is from Li et al. (2008). (b) Location of Dronning Maud Land (DML) in East Antarctica and the Na-Na Belt in South Africa in Gondwana (after Jacobs et al., 2017). Abbreviations: C, Coats Land; cDML, central Dronning Maud Land; EH, Ellsworth-Haag; F, Filchnerblock; FI, Falkland Islands; FMA, Forster Magnetic Anomaly; G, Grunehogna Craton; GAM, Gamburtsev Mts.; Ki, Kibaran; M, Madagascar; MCRS, Mid Continental Rift System; N, Napier Complex; NC, Nampula Complex; Na-Na, Namaqua-Natal Belt; R, Read Block; TAM, Transantarctic Mts.; V, Vohibori; VCB, Valkyrie Cratonic Block.

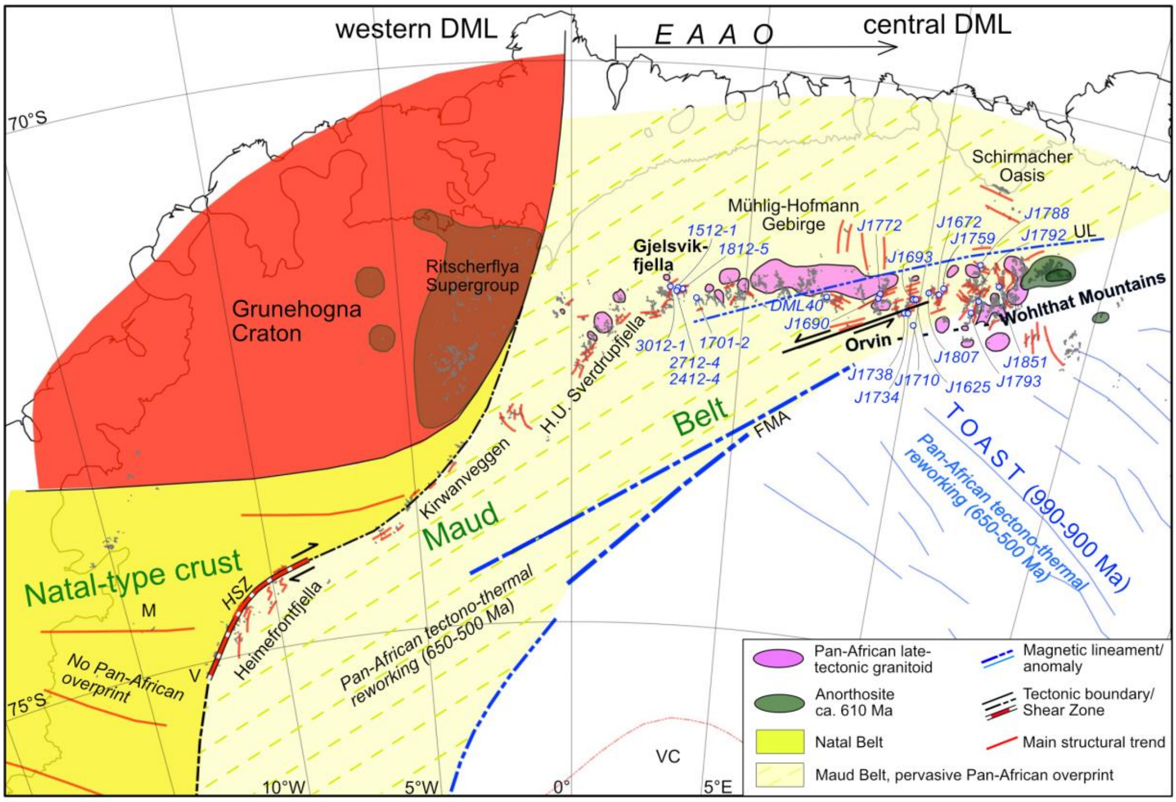

Fig. 2: Geological overview map of the study area and sample localities in the Orvin-Wohlthat Mountains and Gjelsvikfjella, cDML (cDML: from Gjelsvikfjella to Wohlthat mountains in this study). Abbreviations: FMA, Forster magnetic anomaly; HSZ, Heimefront Shear Zone; M, Mannefallknausane; TOAST, Tonian Oceanic Arc Super Terrane; UL, Ulvetanna Lineament; V, Vardeklettane Terrane.

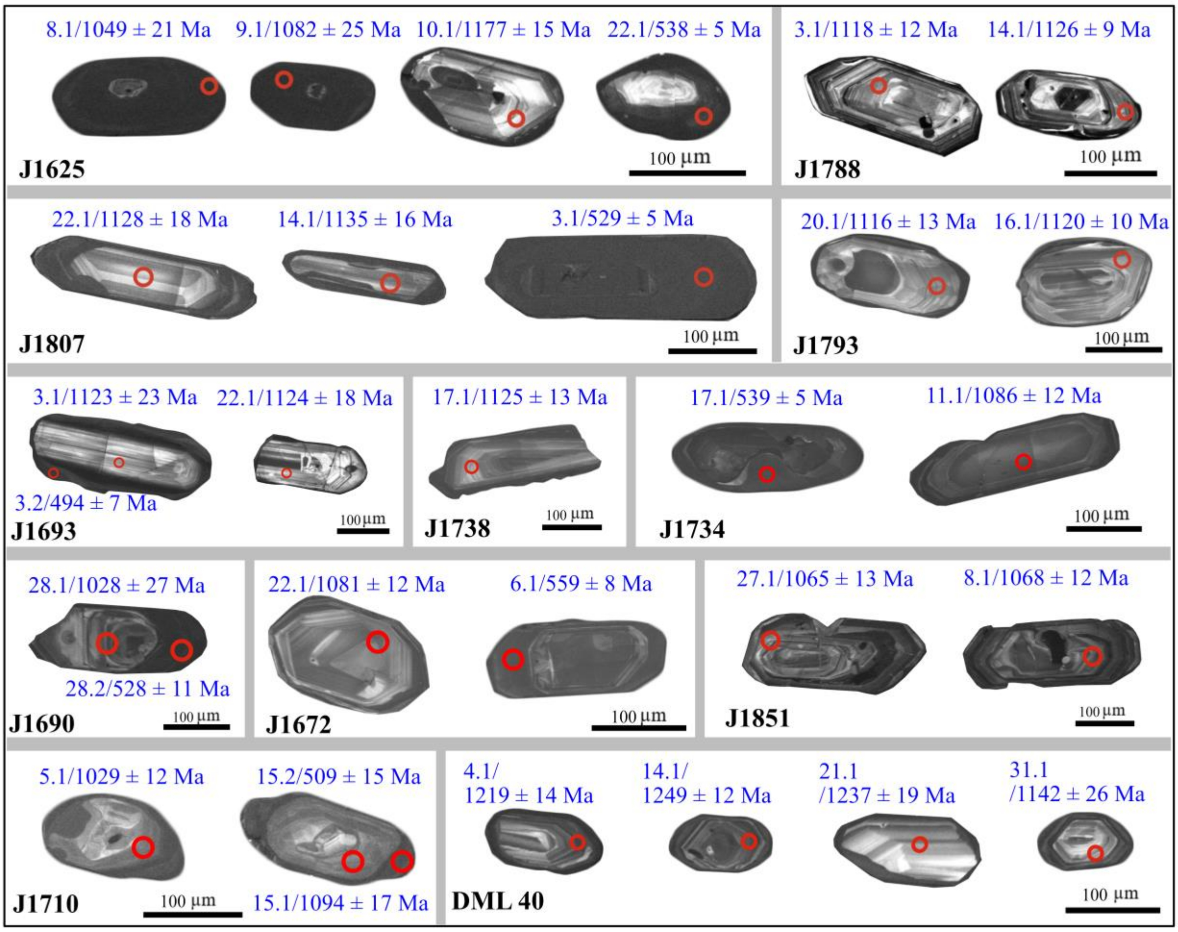

Fig. 3: Representative CL images with $^{206}Pb/^{238}U$ ages of zircons from the Orvin-Wohlthat Mountains.

899

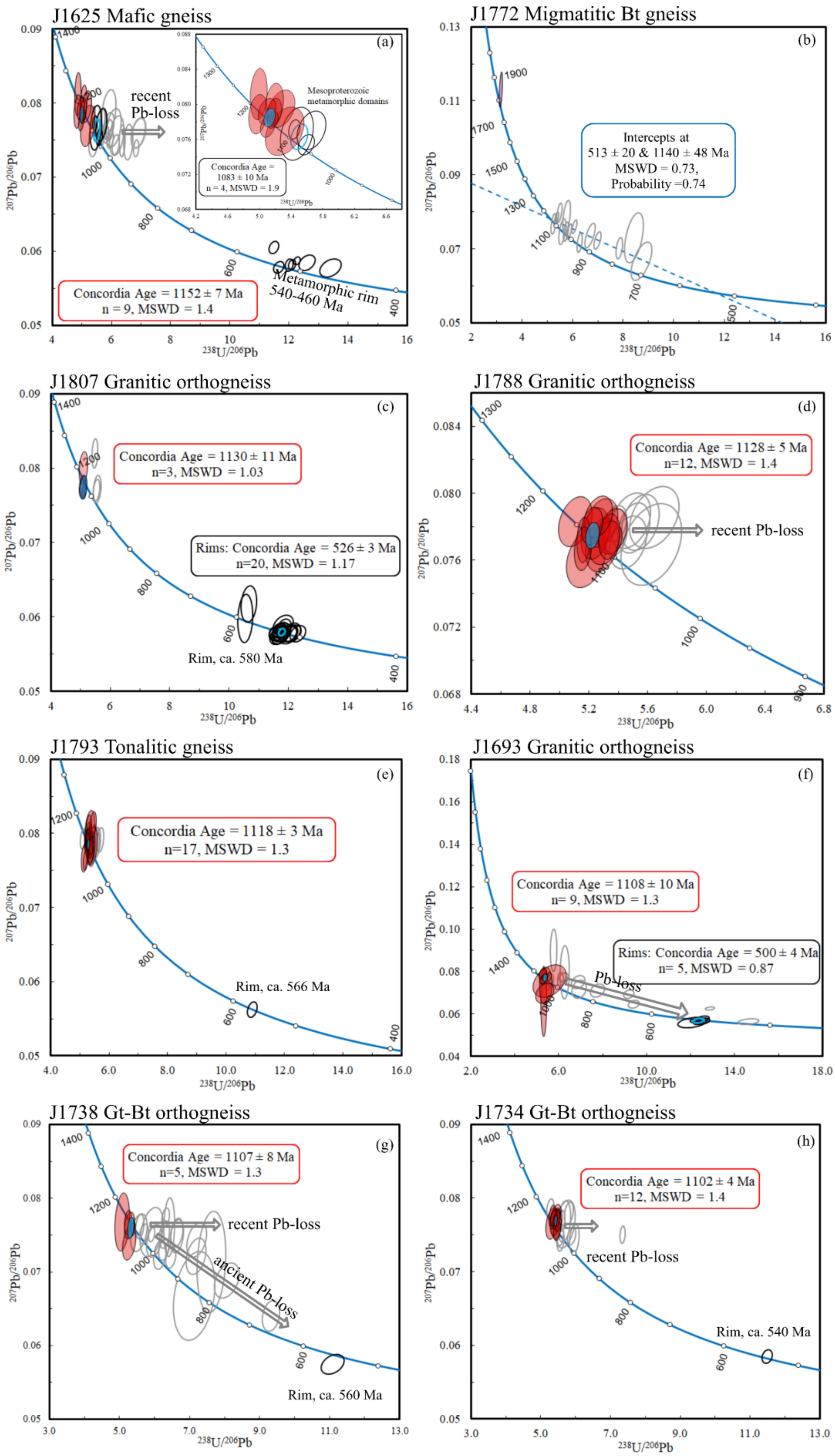

J1625 Mafic gneiss
(a)
recent Pb-loss
Mesoproterozoic metamorphic domains
Concordia Age = 1083 ± 10 Ma n = 4, MSWD = 1.9
Metamorphic rim 540-460 Ma
Concordia Age = 1152 ± 7 Ma n = 9, MSWD = 1.4
J1772 Migmatitic Bt gneiss
(b)
Intercepts at 513 ± 20 & 1140 ± 48 Ma MSWD = 0.73, Probability =0.74
J1807 Granitic orthogneiss
(c)
Concordia Age = 1130 ± 11 Ma n=3, MSWD = 1.03
Rims: Concordia Age = 526 ± 3 Ma n=20, MSWD = 1.17
Rim, ca. 580 Ma
J1788 Granitic orthogneiss
(d)
Concordia Age = 1128 ± 5 Ma n=12, MSWD = 1.4
recent Pb-loss
J1793 Tonalitic gneiss
(e)
Concordia Age = 1118 ± 3 Ma n=17, MSWD = 1.3
Rim, ca. 566 Ma
J1693 Granitic orthogneiss
(f)
Concordia Age = 1108 ± 10 Ma n= 9, MSWD = 1.3
Rims: Concordia Age = 500 ± 4 Ma n= 5, MSWD = 0.87
Pb-loss
J1738 Gt-Bt orthogneiss
(g)
Concordia Age = 1107 ± 8 Ma n=5, MSWD = 1.3
recent Pb-loss
ancient Pb-loss
Rim, ca. 560 Ma
J1734 Gt-Bt orthogneiss
(h)
Concordia Age = 1102 ± 4 Ma n=12, MSWD = 1.4
recent Pb-loss
Rim, ca. 540 Ma

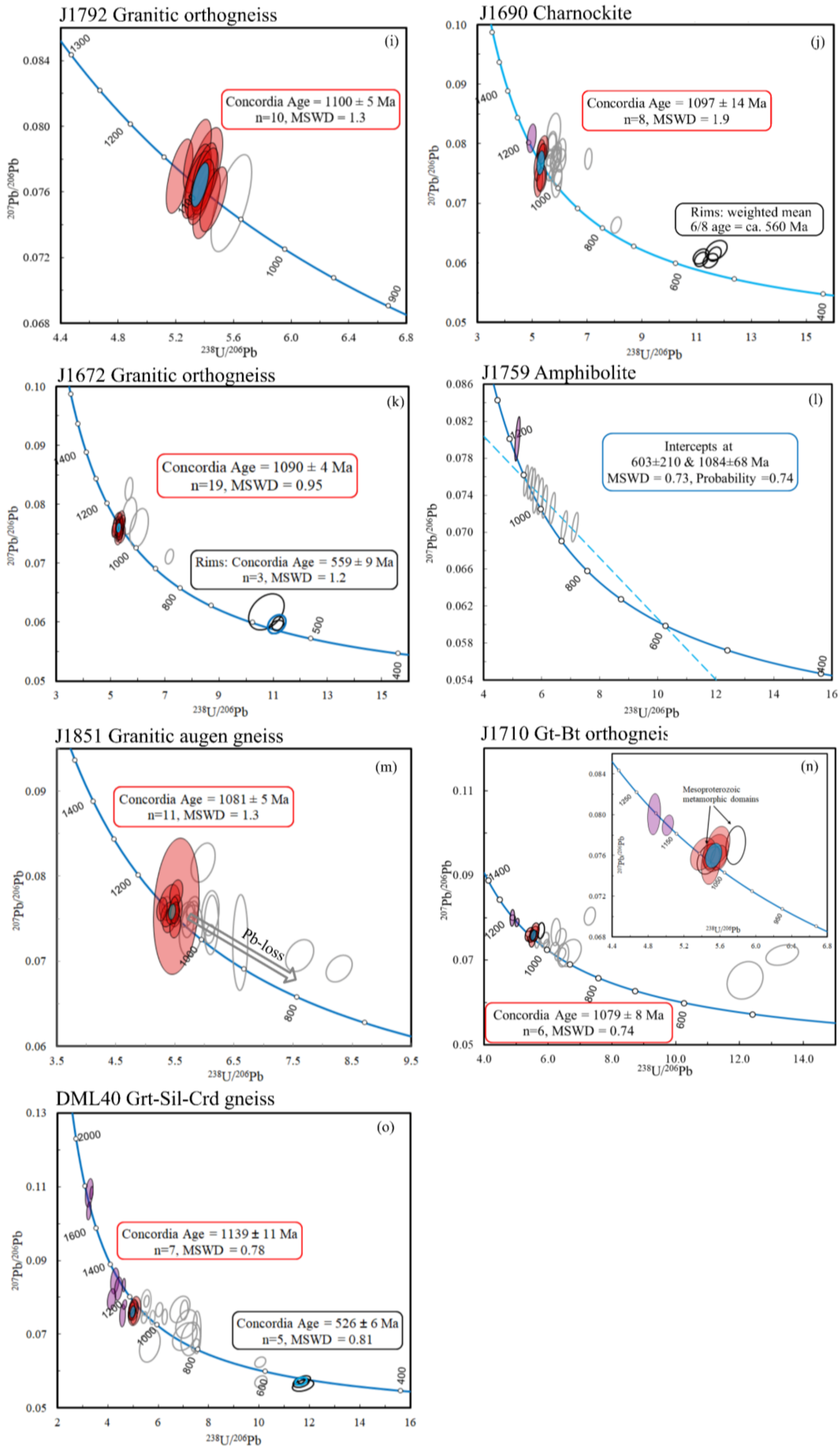
J1792 Granitic orthogneiss
(i)
Concordia Age = 1100 ± 5 Ma
n=10, MSWD = 1.3
J1690 Charnockite
(j)
Concordia Age = 1097 ± 14 Ma
n=8, MSWD = 1.9
Rims: weighted mean
6/8 age = ca. 560 Ma
J1672 Granitic orthogneiss
(k)
Concordia Age = 1090 ± 4 Ma
n=19, MSWD = 0.95
Rims: Concordia Age = 559 ± 9 Ma
n=3, MSWD = 1.2
J1759 Amphibolite
(l)
Intercepts at
603±210 & 1084±68 Ma
MSWD = 0.73, Probability =0.74
J1851 Granitic augen gneiss
(m)
Concordia Age = 1081 ± 5 Ma
n=11, MSWD = 1.3
Pb-loss
J1710 Gt-Bt orthogneis
(n)
Mesoproterozoic
metamorphic domains
Concordia Age = 1079 ± 8 Ma
n=6, MSWD = 0.74
DML40 Grt-Sil-Crd gneiss
(o)
Concordia Age = 1139 ± 11 Ma
n=7, MSWD = 0.78
Concordia Age = 526 ± 6 Ma
n=5, MSWD = 0.81
$^{207}Pb/^{206}Pb$
$^{238}U/^{206}Pb$

Fig. 4: U-Pb zircon geochronology of samples from Orvin-Wohlthat Mountains. Purple: inherited zircons and detrital zircons in DML 40; Red: Grenville-age concordant igneous zircons with concordia ellipse (blue); Black: Grenville-age and Pan-African metamorphic zircons; Grey: discordant zircon. Error ellipses shown at 2σ level.

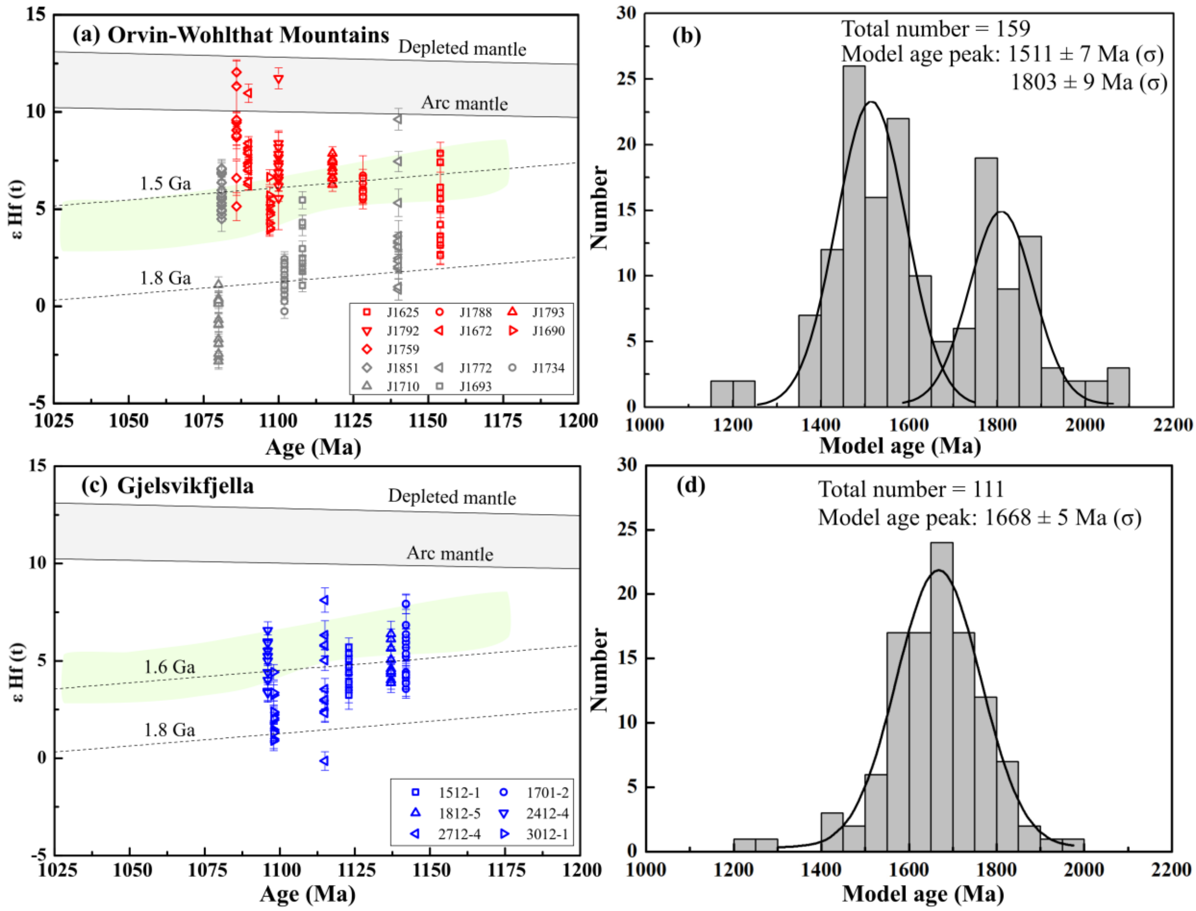

Fig. 5: Time versus ε_{Hf} (t) plot and histograms of zircon Hf model ages from the Orvin-Wohlthat Mountains (a, b) and Gjelsvikfjella (c, d). The evolution curve of arc mantle is from Dhuime et al. (2011). The light green range is composed of samples from the Natal Belt (Spencer et al., 2015). Samples from the Orvin-Wohlthat Mountains with moderate $\delta^{18}O$ values (5.5–7.1 ‰) and juvenile Hf isotopic compositions are marked in red; the dark grey samples have evolved Hf and/or elevated O isotopic composition (a). These samples display two model age peaks at the Meso- and Paleoproterozoic times respectively (b). The Gjelsvikfjella samples have more evolved Hf isotopic composition than juvenile samples from the Orvin-Wohlthat Mountains with a cluster of model ages in late

Paleoproterozoic times (c, d). Evolution curves of continental crust are calculated by assuming a $^{176}Lu/^{177}Hf$ ratio of 0.015.

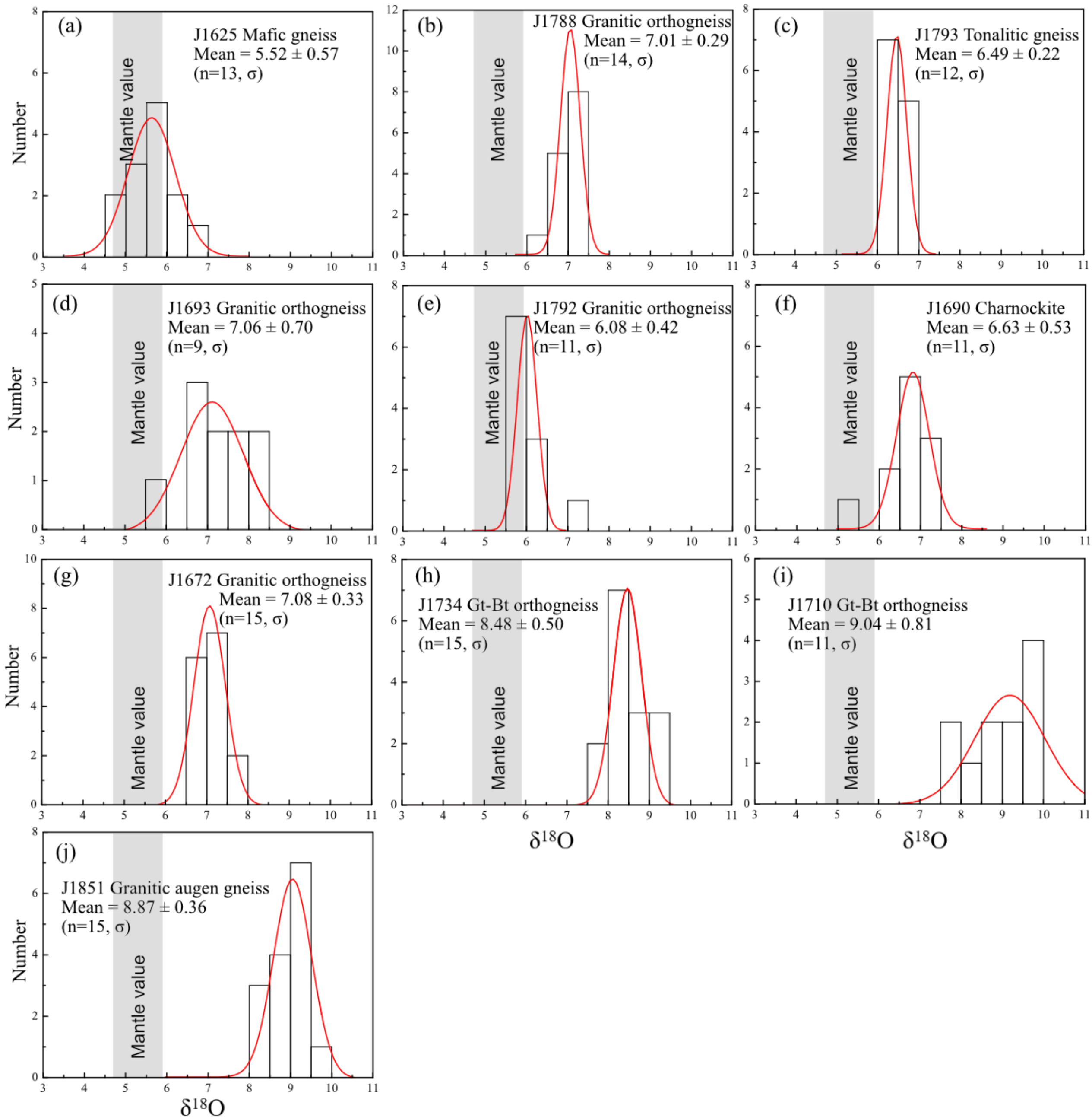

Fig. 6: Histograms of $\delta^{18}O$ values of samples from the Orvin-Wohlthat Mountains.

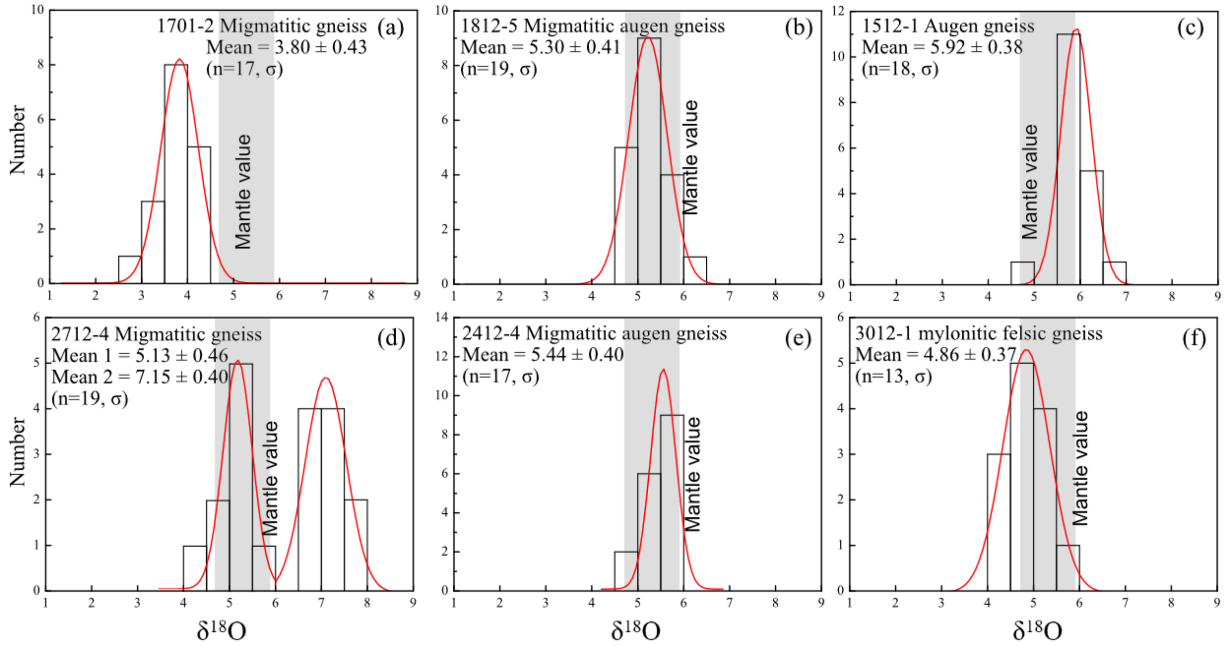

Fig. 7: Histograms of $\delta^{18}O$ values of samples from the Gjelsvikfjella.

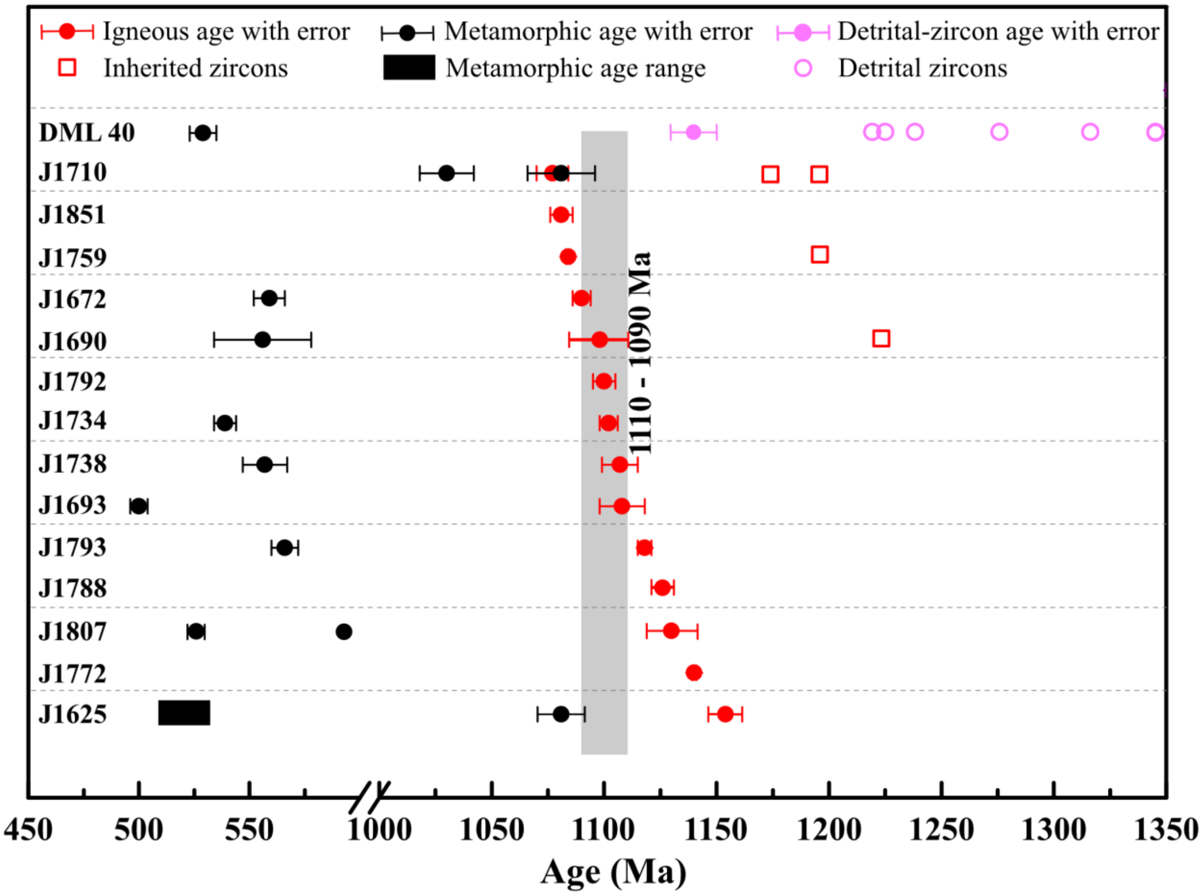

Fig. 8: Summary of Mesoproterozoic ages from igneous and detrital zircons and Pan-African metamorphic time in this study, with an igneous age concentration at 1110–1090 Ma (grey vertical bar).

Sample 1772 and 1759 are marked with approximate upper-intercept age without error bars.

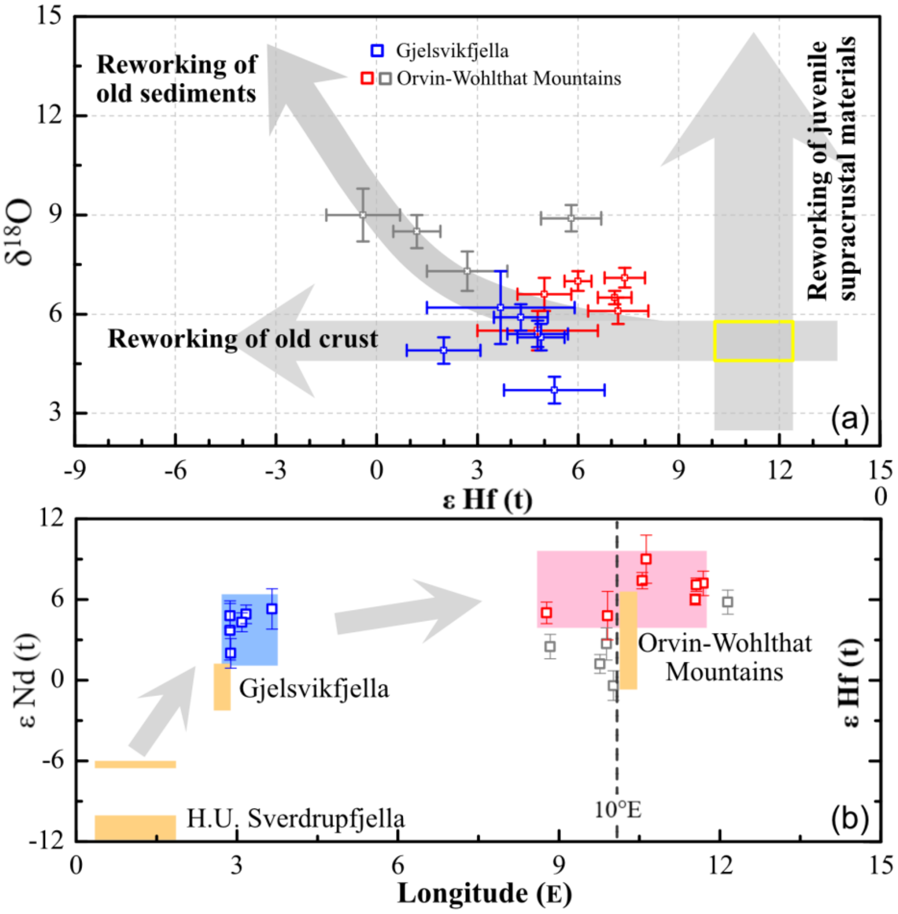

Fig. 9: (a) Plot of $\delta^{18}O$ versus ε_{Hf} (t) for zircons from cDML, showing the difference in source composition of samples between Gjelsvikfjella and the Orvin-Wohlthat Mountains. The yellow rectangles show the theoretical Hf-O isotopic composition of 1.1 Ga arc- and depleted-mantle derived magmas ($\delta^{18}O$ = 4.7–5.9 ‰, ε_{Hf} (t) = +10– (+)12.5). The old basement and sediments are assumed to be Paleoproterozoic, with similarly evolved Hf isotopic composition but mantle-like and high $\delta^{18}O$ values respectively. Most samples from the Orvin-Wohlthat Mountains (red) are rather juvenile with moderate $\delta^{18}O$ values and high ε_{Hf} (t) values. Some samples (dark grey) display an elevated O isotopic signature associated with much lower ε_{Hf} (t) values, indicating the involvement of older Paleoproterozoic sediments. Mantle-like O and more evolved Hf isotopic compositions of samples from Gjelsvikfjella (blue) indicate the addition of old basements in the source. (b) ε_{Hf} (t) and ε_{Nd} (t) vs. longitude diagram showing the increasingly juvenile isotopic composition towards the east, away from the Grunehogna Craton. The orange rectangles show ε_{Nd} values reported by Wareham et al. (1998), Jacobs et al. (1998),

Paulsson and Austrheim (2003) and Grosch et al. (2007).

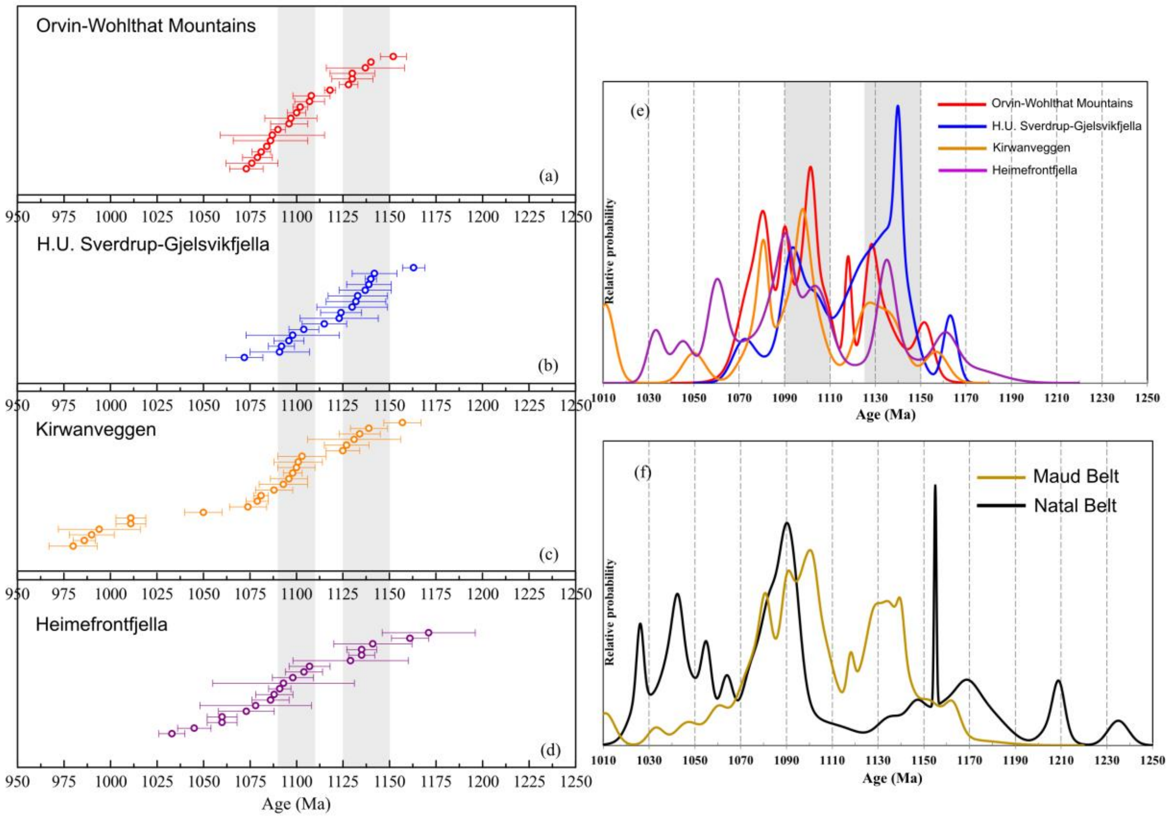

Fig. 10: (a-e) Summary of igneous U-Pb zircon ages from different parts of the Maud Belt. Two main periods of magmatism (1150–1125 Ma, 1110–1090 Ma) are marked with grey bar; (f) Comparison of major times of igneous activity in the Maud and Natal belts. The Natal Belt has an early crustal record that is several tens of million years older than the Maud Belt. The 1150–1120 Ma igneous ages are interpreted as continental-arc magmatism in the Maud Belt, while this time period was almost quiet in Natal. (Sources for the data of the Orvin-Wohlthat Mountains: Jacobs et a., 1998, Baba et al., 2015; and data in this study; H.U. Sverdrup-Gjelsvikfjella: Paulsson and Austrheim, 2003; Jacobs et al., 2003a, c, 2008; Board et al., 2004; Bisnath et al., 2006; Grantham et al., 2011; Hokada et al., 2019; Kirwanveggen: Harris et al., 1995; Harris, 1999; Jackson, 1999; Heimefrontfjella: Arndt et al., 1991; Bauer et al., 2003a, b; Jacobs et al., 2003b; Natal: Thomas and Eglington, 1990; Thomas et al., 1993, 1999, 2003; Johnston et al., 2001; Mendonidis and Armstrong, 2009, 2016; Mendonidis et al., 2002, 2009, 2015; Eglington et al., 2003, 2010; Spencer et al., 2015; Hokada et al., 2019).

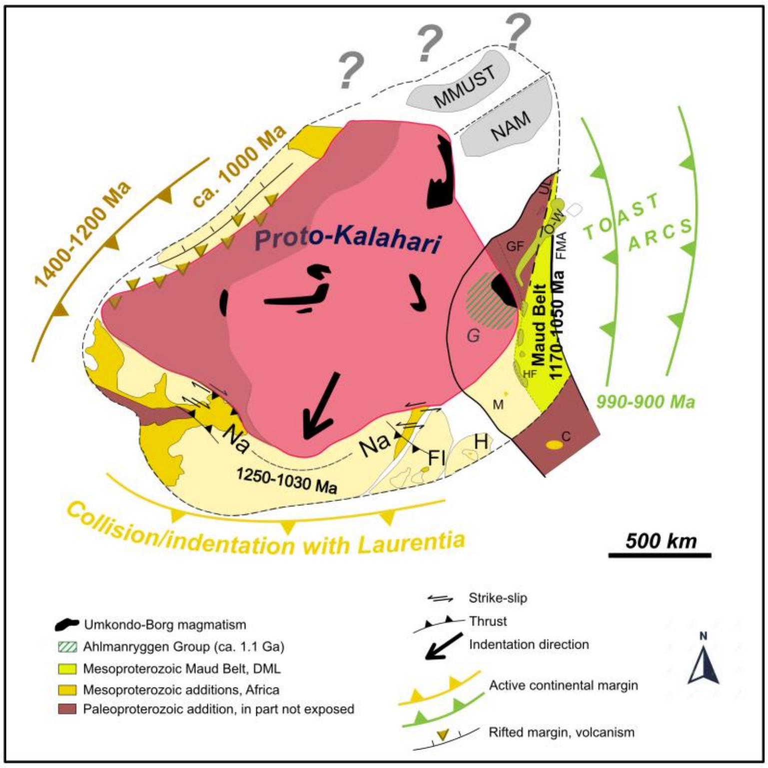

Fig. 11: Tectonic setting along the margin of the Proto-Kalahari Craton in late Mesoproterozoic times (modified from Jacobs et al., 2008a). The eastern margin along the Maud Belt is interpreted as an active continental margin with ancient continental crust most likely extending to cDML. The southern margin, in contrast, is characterized by outward subduction with accretion of Proterozoic arcs or microcontinents followed by collision with Laurentia to form the Na-Na Belt. Abbreviations: C, Coats Land Block; O-W, Orvin-Wohlthat Mountains; FMA, Forster Magnetic Anomaly; FI, Falkland Islands; G, Grunehogna Craton; GF, Gjelsvikfjella; H, Haag Nunatak; HF, Heimefrontfjella; M, Mannefallknausane; MMUST, Marupa-Malawi-Unango south Tanzania terrane; NAM, Nampula Complex; UL, Ulvetanna Lineament.

References

Amelin, Y., Lee, D.C., Halliday, A.N., Pidgeon, R.T., 1999. Nature of the Earth's earliest crust from hafnium isotopes in single detrital zircons. Nature 399, 252–255.

Arndt, N.T., Todt, W., Chauvel, C., Tapfer, M., Weber, K., 1991. U-Pb zircon age and Nd isotopic composition of granitoids, charnockites and supracrustal rocks from Heimefrontfjella, Antarctica. Geologische Rundschau 80, 759–777.

Baba, S., Horie, K., Hokada, T., Owada, M., Adachi, T., Shiraishi, K., 2015. Multiple collisions in the East African–Antarctica Orogen: constraints from timing of metamorphism in the Filchnerfjella and Hochlinfjellet terranes in central Dronning Maud Land. The Journal of Geology 123, 55–77.

Barton, J.M., Klemd, R., Allsopp, H.L., Auret, S.H., Copperthwaite, Y.E., 1987. The geology and geochronology of the Annandagstoppane granite, western Dronning Maud Land, Antarctica. Contributions to Mineralogy and Petrology 97, 488–496.

Bauer, W., Jacobs, J., Fanning, C.M., Schmidt, R., 2003a. Late Mesoproterozoic Arc and Back-arc Volcanism in the Heimefrontfjella (East Antarctica) and Implications for the Palaeogeography at the Southeastern Margin of the Kaapvaal-Grunehogna Craton. Gondwana Research 6, 449–465.

Bauer, W., Fielitz, W., Jacobs, J., Fanning, C.M., Spaeth, G., 2003b. Mafic dykes from Heimefrontfjella and implications for the post-Grenvillian to pre-Pan-African geological evolution of western Dronning Maud Land, Antarctica. Antarctic Science 15, 379–391.

Bauer, W., Thomas, R.J., Jacobs, J., 2003c. Proterozoic-Cambrian history of Dronning Maud Land in the context of Gondwana assembly. Geological Society, London, Special Publication 206, 247–269.

Bauer, W., Jacobs, J., Thomas, R.J., Spaeth, G., Weber, K., 2009. Geology of the Vardeklettane Terrane, Heimefrontfjella (East Antarctica). Polarforschung 79, 29–32.

Bindeman, I.N., Eiler, J.M., Yogodzinski, G.M., Tatsumi, Y., Stern, C.R., Grove, T.L., Portnyagin, M., Hoernle, K., Danyushevsky, L.V., 2005. Oxygen isotope evidence for slab melting in modern and ancient subduction zones. Earth and Planetary Science Letters 235, 480–496.

Bingen, B., Nordgulen, Ø., Viola, G., 2008. A four-phase model for the Sveconorwegian orogeny, SW Scandinavia. Norwegian Journal of Geology 88, 43–72.

Bingen, B., Jacobs, J., Viola, G., Henderson, I.H.C., Skår, Ø., Boyd, R., Thomas, R.J., Solli, A., Key, R.M., Daudi, E.X.F., 2009. Geochronology of the Precambrian crust in the Mozambique belt in NE Mozambique, and implications for Gondwana assembly. Precambrian Research 170, 231–255.

Bingen, B., Viola, G., 2018. The early-Sveconorwegian orogeny in southern Norway: Tectonic model involving delamination of the sub-continental lithospheric mantle. Precambrian Research 313, 170–204.

Bisnath, A., Frimmel, H.E., Armstrong, R.A., Board, W.S., 2006. Tectono-thermal evolution of the Maud Belt: New SHRIMP U–Pb zircon data from Gjelsvikfjella, Dronning Maud Land, East Antarctica. Precambrian Research 150, 95–121.

Black, L.P., Kamo, S.L., Allen, C.M., Davis, D.W., Aleinikoff, J.N., Valley, J.W., Mundil, R., Campbell, I.H., Korsch, R.J., Williams, I.S., Foudoulis, C., 2004. Improved ^{206}Pb/^{238}U microprobe geochronology by the monitoring of a trace-element-related matrix effect; SHRIMP, ID–TIMS, ELA–ICP–MS and oxygen isotope documentation for a series of zircon standards. Chemical Geology 205, 115–140.

Board, W.S., Frimmel, H.E., Armstrong, R.A., 2005. Pan-African Tectonism in the Western Maud Belt: P–T–t Path for High-grade Gneisses in the H.U. Sverdrupfjella, East Antarctica. Journal of Petrology 46, 671-699.

Boekhout, F., Roberts, N.M., Gerdes, A., Schaltegger, U., 2015. A Hf-isotope perspective on continent formation in the south Peruvian Andes. Geological Society, London, Special Publication 389, 305–321.

Bouvier, A., Vervoort, J.D., Patchett, P.J., 2008. The Lu–Hf and Sm–Nd isotopic composition of CHUR: constraints from unequilibrated chondrites and implications for the bulk composition of terrestrial planets. Earth and Planetary Science Letters 273, 48–57.

Ernst, R.E., Pereira, E., Hamilton, M.A., Pisarevsky, S.A., Rodriques, J., Tassinari, C.C., Teixeira, W., Van-Dunem, V., 2013. Mesoproterozoic intraplate magmatic 'barcode' record of the Angola portion of the Congo Craton: Newly dated magmatic events at 1505 and 1110 Ma and implications for Nuna (Columbia) supercontinent reconstructions. Precambrian Research 230, 103–118.

Cawood, P.A., Kröner, A., Collins, W.J., Kusky, T.M., Mooney, W.D., Windley, B.F., 2009. Accretionary orogens through Earth history. Geological Society, London, Special Publication 318, 1–36.

Cawood, P.A., Strachan, R.A., Pisarevsky, S.A., Gladkochub, D.P., Murphy, J.B., 2016. Linking collisional and accretionary orogens during Rodinia assembly and breakup: Implications for models of supercontinent cycles. Earth and Planetary Science Letters 449, 118–126.

Cawood, P.A., Pisarevsky, S.A., 2017. Laurentia-Baltica-Amazonia relations during Rodinia assembly. Precambrian Research 292, 386–397.

Chapman, J.B., Ducea, M.N., Kapp, P., Gehrels, G.E., DeCelles, P.G., 2017. Spatial and temporal radiogenic isotopic trends of magmatism in Cordilleran orogens. Gondwana Research 48, 189–204.

Collins, W.J., Belousova, E.A., Kemp, A.I., Murphy, J.B., 2011. Two contrasting Phanerozoic orogenic systems revealed by hafnium isotope data. Nature Geoscience 4, 333–337.

Condie, K.C., 2005. Earth as an Evolving Planetary System. Elsevier, Amsterdam, Netherlands, 90–91.

Dalziel, I.W., Mosher, S., Gahagan, L.M., 2000. Laurentia-Kalahari collision and the assembly of Rodinia. The Journal of Geology 108, 499–513.

Davis, D.W., Green, J.C., 1997. Geochronology of the North American Midcontinent rift in western Lake Superior and implications for its geodynamic evolution. Canadian Journal of Earth Sciences 34, 476–488.

De Kock, M.O., Ernst, R., Söderlund, U., Jourdan, F., Hofmann, A., Le Gall, B., Bertrand, H., Chisonga, B.C., Beukes, N., Rajesh, H.M., Moseki, L.M., 2014. Dykes of the 1.11 Ga Umkondo LIP, Southern Africa: clues to a complex plumbing system. Precambrian Research 249, 129–143.

Dhuime, B., Hawkesworth, C., Cawood, P., 2011. When continents formed. Science 331, 154–155.

Ducea, M.N., Saleeby, J.B., Bergantz, G., 2015. The architecture, chemistry, and evolution of continental magmatic arcs. Annual Review of Earth and Planetary Sciences 43, 299–331.

Eiler, J.M., 2001. Oxygen isotope variations of basaltic lavas and upper mantle rocks. Reviews in Minerology and Geochemistry 43, 319–364.

Eglington, B.M., Harmer, R.E., Kerr, A., 1989. Isotope and geochemical constraints on Proterozoic crustal evolution in south-eastern Africa. Precambrian Research. 45, 159–174.

Eglington, B.M., Thomas, R.J., Armstrong, R.A., Walraven, F., 2003. Zircon geochronology of the Oribi Gorge Suite, KwaZulu-Natal, South Africa: Constraints on the timing of trans-current shearing in the Namaqua–Natal Belt. Precambrian Research 123, 29–46.

Eglington, B.M., Thomas, R.J., Armstrong, R.A., 2010. U-Pb SHRIMP zircon dating of Mesoproterozoic magmatic rocks from the Scottburgh area, central Mzumbe Terrane, KwaZulu-Natal, South Africa. South African Journal of Geology 113, 229–235.

Elburg, M.A., van Bergen, M.J., Hoogewerff, J., Foden, J., Vroon, P.Z., Zulkarnain, I., Nasution, A., 2002. Geochemical trends across an arc-continent collision zone: magma sources and slab-wedge transfer processes below the Pantar Strait volcanoes (Indonesia). Geochimica et Cosmochimica Acta 66, 2771–2789.

Elburg, M., Jacobs, J., Andersen, T., Clark, C., Läufer, A., Ruppel, A., Krohne, N., Damaske, D., 2015. Early Neoproterozoic metagabbro-tonalite-trondhjemite of Sør Rondane (East Antarctica): Implications for supercontinent assembly. Precambrian Research 259, 189–206.

Ernst, R.E., Pereira, E., Hamilton, M.A., Pisarevsky, S.A., Rodriques, J., Tassinari, C.C., Teixeira, W., Van-Dunem, V., 2013. Mesoproterozoic intraplate magmatic 'barcode' record of the Angola portion of the Congo Craton: Newly dated magmatic events at 1505 and 1110 Ma and implications for Nuna (Columbia) supercontinent reconstructions. Precambrian Research 230, 103–118.

Frimmel, H.E., 2004. Formation of a late Mesoproterozoic supercontinent: the South Africa–East Antarctica connection. In: Eriksson, P.G., Altermann, W., Nelson, D.R., Mueller, W.U., Catuneanu, O. (Eds.), The Precambrian Earth: Tempos and Events. Developments in Precambrian Geology, 12, 240–255.

Gaucher, C., Frei, R., Chemale, F., Frei, D., Bossi, J., Martínez, G., Chiglino, L., Cernuschi, F., 2011. Mesoproterozoic evolution of the Río de la Plata Craton in Uruguay: at the heart of Rodinia? International Journal of Earth Sciences 100, 273–288.

Godard, G., Palmeri, R., 2013. High-pressure metamorphism in Antarctica from the Proterozoic to the Cenozoic: A review and geodynamic implications. Gondwana Research 23, 844–864.

Golynsky, A., Jacobs, J., 2001. Grenville-age versus pan-african magnetic anomaly imprints in Western Dronning Maud Land, East Antarctica. The Journal of Geology 109, 136–142.

Gose, W.A., Helper, M.A., Connelly, J.N., Hutson, F.E., Dalziel, I.W., 1997. Paleomagnetic data and U‐Pb isotopic age determinations from Coats Land, Antarctica: Implications for late Proterozoic plate reconstructions. Journal of Geophysical Research: Solid Earth, 102(B4), 7887–7902.

Gose, W.A., Hanson, R.E., Dalziel, I.W., Pancake, J.A., Seidel, E.K., 2006. Paleomagnetism of the 1.1 Ga Umkondo large igneous province in southern Africa. Journal of Geophysical Research: Solid Earth, 111(B9), 1–18.

Grantham, G.H., 1992. Geological evolution of western H.U. Sverdrupfjella, Dronning Maud Land, Antarctica (Doctoral dissertation, University of Natal).

Grantham, G.H., Storey, B.C., Thomas, R.J., Jacobs, J., Ricci, C.A., 1997. The pre-break-up position of Haag Nunataks within Gondwana: possible correlatives in Natal and Dronning Maud Land. The Antarctic Region: Geological Evolution and Processes. Terra Antartica Publication, Siena, 13–20.

Grantham, G.H., Eglington, B.M., Thomas, R.J., Mendonidis, P., 2001. The Nature of the Grenville-age Charnockitic A-type Magmatism from the Natal, Namaqua and Maud Belts of Southern Africa and Western Dronning Maud Land, Antarctica. National Institute of Polar Research, Tokyo (Special Issue 55), 59–86.

Grantham, G.H., Manhica, A.D.S.T., Armstrong, R.A., Kruger, F.J., Loubser, M., 2011. New SHRIMP, Rb/Sr and Sm/Nd isotope and whole rock chemical data from central Mozambique and western Dronning Maud Land, Antarctica: Implications for the nature of the eastern margin of the Kalahari Craton and the amalgamation of Gondwana. Journal of African Earth Sciences 59, 74–100.

Griffin, W.L., Pearson, N.J., Belousova, E., Jackson, S.E., van Achterbergh, E., O'Reilly, S.Y., Shee, S.R., 2000. The Hf isotope composition of cratonic mantle: LAM-MC-ICPMS analysis of zircon megacrysts in kimberlites. Geochimica et Cosmochimica Acta 64, 133–147.

Groenewald, P.B., Moyes, A.B., Grantham, G.H., Krynauw, J.R., 1995. East Antarctic crustal evolution: geological constraints and modelling in western Dronning Maud Land, East Antarctica. Precambrian Research 75, 231–250.

Grosch, E.G., Bisnath, A., Frimmel, H.E., Board, W.S., 2007. Geochemistry and tectonic setting of mafic rocks in western Dronning Maud Land, East Antarctica: implications for the geodynamic evolution of the Proterozoic Maud Belt. Journal of the Geological Society 164, 465–475.

Grosch, E.G., Frimmel, H.E., Abu-Alam, T., Košler, J., 2015. Metamorphic and age constraints on crustal reworking in the western H.U. Sverdrupfjella: implications for the evolution of western Dronning Maud Land, Antarctica. Journal of the Geological Society 172, 499–518.

Hagen-Peter, G., Cottle, J., 2017. Evaluating the relative roles of crustal growth versus reworking through continental arc magmatism: A case study from the Ross orogen, Antarctica. Gondwana Research 55, 153–156.

Hanson, R.E., Martin, M.W., Bowring, S.A., Munyanyiwa, H., 1998. U-Pb zircon age for the Umkondo dolerites, eastern Zimbabwe: 1.1 Ga large igneous province in southern Africa–East Antarctica and possible Rodinia correlations. Geology 26, 1143–1146.

Hanson, R.E., Crowley, J.L., Bowring, S.A., Ramezani, J., Gose, W.A., Dalziel, I.W., Pancake, J.A., Seidel, E.K., Blenkinsop, T.G., Mukwakwami, J., 2004. Coeval large-scale magmatism in the Kalahari and Laurentian cratons during Rodinia assembly. Science 304, 1126–1129.

Harris, P.D., Moyes, A.B., Fanning, C.M., Arimstrong, R.A., 1995. Zircon Ion microscope results from the Maudheim high-grade gneiss terrane, western Dronning Maud Land, Antarctica. Extended Abstracts, Centennial Geocongress, Rand Afrikaans University, Johannesburg, 240–243.

Harris, P.D. 1999. The geological evolution of Neumayerskarvet in the northern Kirwanveggen, western Dronning Maud Land, Antarctica. Unpublished. Ph.D. thesis, Rand Afrikaans University.

Hawkesworth, C.J., Kemp, A.I.S., 2006. Using hafnium and oxygen isotopes in zircons to unravel the record of crustal evolution. Chemical Geology 226, 144–162.

Heinonen, A.P., Andersen, T., Rämö, O.T., 2010. Re-evaluation of rapakivi petrogenesis: Source constraints from the Hf isotope composition of zircon in the rapakivi granites and associated mafic rocks of southern Finland. Journal of Petrology 51, 1687–1709.

Hokada, T., Grantham, G.H., Arima, M., Saito, S., Shiraishi, K., Armstrong, R.A., Eglington, B., Misawa, K., Kaiden, H., 2019. Stenian A-type granitoids in the Namaqua-Natal Belt, southern Africa, Maud Belt, Antarctica and Nampula Terrane, Mozambique: Rodinia and Gondwana amalgamation implications. Geoscience Frontiers 10, 2265–2280.

Hiess, J., Bennett, V.C., Nutman, A.P., Williams, I.S., 2011. Archaean fluid-assisted crustal cannibalism recorded by low $\delta^{18}O$ and negative ε Hf (T) isotopic signatures of West Greenland granite zircon. Contributions to Mineralogy and Petrology 161, 1027–1050.

Hynes, A., Rivers, T., 2010. Protracted continental collision—Evidence from the Grenville orogen. Canadian Journal of Earth Sciences 47, 591–620.

Iizuka, T., Campbell, I.H., Allen, C.M., Gill, J.B., Maruyama, S., Makoka, F., 2013. Evolution of the African continental crust as recorded by U–Pb, Lu–Hf and O isotopes in detrital zircons from modern rivers. Geochimica et Cosmochimica Acta 107, 96–120.

Jacobs, J., Thomas, R.J., Weber, K., 1993. Accretion and indentation tectonics at the southern edge of the Kaapvaal craton during the Kibaran (Grenville) orogeny. Geology 21, 203–206.

Jacobs, J., Bauer, W., Spaeth, G., Thomas, R.J., Weber, K., 1996. Lithology and structure of the Grenville-aged ($\approx$ 1.1 Ga) basement of heimefrontfjella (East Antarctica). Geologische Rundschau 85, 800–821.

Jacobs, J., Thomas, R.J., Armstrong, R.A., Henjes-Kunst, F., 1999. Age and thermal evolution of the Mesoproterozoic Cape Meredith Complex, West Falkland. Journal of the Geological Society 156, 917–928.

Jacobs, J., Fanning, C.M., Henjes-Kunst, F., Olesch, M., Paech, H.J., 1998. Continuation of the Mozambique Belt into East Antarctica: Grenville-age metamorphism and polyphase Pan-African high-grade events in central Dronning Maud Land. The Journal of Geology 106, 385–406.

Jacobs, J., Bauer, W., Fanning, C.M., 2003a. New age constraints for Grenville-age metamorphism in western central Dronning Maud Land (East Antarctica), and implications for the palaeogeography of Kalahari in Rodinia. International Journal of Earth Sciences 92, 301–315.

Jacobs, J., Fanning, C.M., Bauer, W., 2003b. Timing of Grenville-age vs. Pan-African medium- to high grade metamorphism in western Dronning Maud Land (East Antarctica) and significance for correlations in Rodinia and Gondwana. Precambrian Research 125, 1–20.

Jacobs, J., Bauer, W., Fanning, C.M., 2003c. Late Neoproterozoic/Early Palaeozoic events in central Dronning Maud Land and significance for the southern extension of the East African Orogen into East Antarctica. Precambrian Research 126, 27–53.

Jacobs, J., Pisarevsky, S., Thomas, R.J., Becker, T., 2008a. The Kalahari Craton during the assembly and dispersal of Rodinia. Precambrian Research 160, 142–158.

Jacobs, J., Bingen, B., Thomas, R.J., Bauer, W., Wingate, M.T., Feitio, P., 2008b. Early Palaeozoic orogenic collapse and voluminous late-tectonic magmatism in Dronning Maud Land and Mozambique: insights into the partially delaminated orogenic root of the East African–Antarctic Orogen? Geological Society, London, Special Publication 308, 69–90.

Jacobs, J., Elburg, M., Läufer, A., Kleinhanns, I.C., Henjes-Kunst, F., Estrada, S., Ruppel, A.S., Damaske, D., Montero, P., Bea, F., 2015. Two distinct Late Mesoproterozoic/Early Neoproterozoic basement provinces in central/eastern Dronning Maud Land, East Antarctica: The missing link, 15–21°E. Precambrian Research 265, 249–272.

Jacobs, J., Opås, B., Elburg, M.A., Läufer, A., Estrada, S., Ksienzyk, A.K., Damaske, D., Hofmann, M., 2017. Cryptic sub-ice geology revealed by a U-Pb zircon study of glacial till in Dronning Maud Land, East Antarctica. Precambrian Research 294, 1–14.

Jackson, C. 1999. Characterizaton of the Mesoproterozoic to Palaeozoic crustal evolution of western Dronning Maud Land. Study 3: Deformational history and thermochronology of the Kirwanveggen. Unpublished report. Council for Geoscience Open File Report: 1999–0135.

Johansson, Å., 2009. Baltica, Amazonia and the SAMBA connection—1000 million years of neighbourhood during the Proterozoic? Precambrian Research 175, 221–234.

Johnston, S.T., Armstrong, R., Heaman, L., McCourt, S., Mitchell, A., Bisnath, A., Arima, M., 2001. Preliminary U-Pb geochronology of the Tugela terrane, Natal belt, eastern South Africa. National Institute of Polar Research (Japan), Special Issue 55, 40–58.

Jones, D.L., Bates, M.P., Li, Z.X., Corner, B., Hodgkinson, G., 2003. Palaeomagnetic results from the ca. 1130 Ma Borgmassivet intrusions in the Ahlmannryggen region of Dronning Maud Land, Antarctica, and tectonic implications. Tectonophysics 375, 247–260.

Jones, R.E., Kirstein, L.A., Kasemann, S.A., Dhuime, B., Elliott, T., Litvak, V.D., Alonso, R., Hinton, R., Facility, E.I.M., 2015. Geodynamic controls on the contamination of Cenozoic arc magmas in the southern Central Andes: Insights from the O and Hf isotopic composition of zircon. Geochimica et Cosmochimica Acta 164, 386–402.

Ksienzyk, A.K., Jacobs, J., 2015. Western Australia-Kalahari (WAlahari) connection in Rodinia: Not supported by U/Pb detrital zircon data from the Maud Belt (East Antarctica) and the Northampton Complex (Western Australia). Precambrian Research 259, 207–221.

Kemp, A.I.S., Hawkesworth, C.J., Foster, G.L., Paterson, B.A., Woodhead, J.D., Hergt, J.M., Gray, C.M., Whitehouse, M.J., 2007. Magmatic and crustal differentiation history of granitic rocks from Hf-O isotopes in zircon. Science 315, 980–983.

Krynauw, J.R., Hunter, D.R., Wilson, A.H., 1988. Emplacement of sills into wet sediments at Grunehogna, western Dronning Maud Land, Antarctica. Journal of the Geological Society 145, 1019–1032.

Lancaster, P.J., Storey, C.D., Hawkesworth, C.J., Dhuime, B., 2011. Understanding the roles of crustal growth and preservation in the detrital zircon record. Earth and Planetary Science Letters 305, 405–412.

Ludwig, K.R., 2011. A Geochronological Toolkit for Microsoft Excel. Berkeley Geochronology Centre Special Publications Version 4.1.

Li, Z.X., Bogdanova, S.V., Collins, A.S., Davidson, A., De Waele, B., Ernst, R.E., Fitzsimons, I.C.W., Fuck, R.A., Gladkochub, D.P., Jacobs, J., Karlstrom, K.E., 2008. Assembly, configuration, and break-up history of Rodinia: a synthesis. Precambrian Research 160, 179–210.

Loewy, S.L., Dalziel, I.W.D., Pisarevsky, S., Connelly, J.N., Tait, J., Hanson, R.E., Bullen, D., 2011. Coats Land crustal block, East Antarctica: A tectonic tracer for Laurentia? Geology 39, 859–862.

Macey, P.H., Thomas, R.J., Grantham, G.H., Ingram, B.A., Jacobs, J., Armstrong, R.A., Roberts, M.P., Bingen, B., Hollick, L., De Kock, G.S., Viola, G., 2010. Mesoproterozoic geology of the Nampula Block, northern Mozambique: Tracing fragments of Mesoproterozoic crust in the heart of Gondwana. Precambrian Research 182, 124–148.

Manhica, A.D.S.T., Grantham, G.H., Armstrong, R.A., Guise, P.G., Kruger, F.J., 2001. Polyphase deformation and metamorphism at the Kalahari Craton—Mozambique Belt boundary. In: Miller, J.A., Holdsworth, R.E., Buick, I.S., Hand, M. (Eds.), Continental Reactivation and Reworking. Geological Society, London, Special Publication 184, 303–322.

Manda, B.W., Cawood, P.A., Spencer, C.J., Prave, T., Robinson, R., Roberts, N.M., 2019. Evolution of the Mozambique Belt in Malawi constrained by granitoid U-Pb, Sm-Nd and Lu-Hf isotopic data. Gondwana Research 68, 93–107.

Marschall, H.R., Hawkesworth, C.J., Storey, C.D., Dhuime, B., Leat, P.T., Meyer, H.P. and Tamm-Buckle, S., 2010. The Annandagstoppane Granite, East Antarctica: evidence for Archaean intracrustal recycling in the Kaapvaal–Grunehogna Craton from zircon O and Hf isotopes. Journal of Petrology 51, 2277–2301.

Marschall, H.R., Hawkesworth, C.J., Leat, P.T., 2013. Mesoproterozoic subduction under the eastern edge of the Kalahari-Grunehogna Craton preceding Rodinia assembly: The Ritscherflya detrital zircon record, Ahlmannryggen (Dronning Maud Land, Antarctica). Precambrian Research 236, 31–45.

McLelland, J.M., Selleck, B.W., Bickford, M.E., Tollo, R.P., Bartholomew, M.J., Hibbard, J.P., Karabinos, P.M., 2010. Review of the Proterozoic evolution of the Grenville Province, its Adirondack outlier, and the Mesoproterozoic inliers of the Appalachians. From Rodinia to Pangea: The Lithotectonic Record of the Appalachian Region: Geological Society of America Memoir 206, 21–49.

McCourt, S., Armstrong, R.A., Grantham, G.H., Thomas, R.J., 2006. Geology and evolution of the Natal belt, South Africa. Journal of African Earth Science 46, 71–92.

Mendonidis, P., Armstrong, R.A., Eglington, B.M., Grantham, G.H., Thomas, R.J., 2002. Metamorphic history and U-Pb Zircon (SHRIMP) geochronology of the Glenmore

Granite: Implications for the tectonic evolution of the Natal Metamorphic Province. South African Journal of Geology 105, 325–336.

Mendonidis, P., Grantham, G.H., 2003. Petrology, origin and metamorphic history of proterozoic-aged granulites of the Natal Metamorphic Province, southeastern Africa. Gondwana Research 6, 607–628.

Mendonidis, P., Armstrong, R.A., Grantham, G.H., 2009. U–Pb SHRIMP ages and tectonic setting of the Munster Suite of the Margate Terrane of the Natal Metamorphic Belt. Gondwana Research 15, 28–37.

Mendonidis, P., Armstrong, R.A., 2009. A new U-Pb zircon age for the Portobello granite from the southern part of the Natal Metamorphic belt. South African Journal of Geology 112, 197–208.

Mendonidis, P., Thomas, R.J., Grantham, G.H., Armstrong, R.A., 2015. Geochronology of emplacement and charnockite formation of the Margate Granite Suite, Natal Metamorphic Province, South Africa: implications for Natal-Maud belt correlations. Precambrian Research 265, 189–202.

Mendonidis, P., Armstrong, R.A., 2016. U–Pb Zircon (SHRIMP) ages of granite sheets and timing of deformational events in the Natal Metamorphic Belt, southeastern Africa: Evidence for deformation partitioning and implications for Rodinia reconstructions. Precambrian Research 278, 22–33.

Mendonidis, P., Thomas, R.J., 2019. A review of the geochronology of the Margate Terrane reveals a history of diachronous terrane docking and arc accretion across the Mesoproterozoic Natal belt, southeastern Africa. Journal of African Earth Sciences 150, 532–545.

Merdith, A.S., Collins, A.S., Williams, S.E., Pisarevsky, S., Foden, J.D., Archibald, D.B., Blades, M.L., Alessio, B.L., Armistead, S., Plavsa, D., Clark, C., 2017. A full-plate global reconstruction of the Neoproterozoic. Gondwana Research 50, 84–134.

Mikhalsky, E., Jacobs, J., 2004. Orthogneisses in central Dronning Maud Land, East Antarctica: their origin and tectonic setting. In: Paech, H.-J. (Ed.), International GeoMaud Expedition of the BGR to Central Dronning Maud in 1995/96–Geological Results, Geologisches Jahrbuch B96, 49–76.

Moabi, N.G., Grantham, G.H., Roberts, J., Le Roux, P., 2017. The geology and geochemistry of the Straumsnutane Formation, Straumsnutane, western Dronning Maud Land, Antarctica and its tectonic setting on the western margin of the Kalahari Craton: additional evidence linking it to the Umkondo Large Igneous Province. Geological Society, London, Special Publication 457, 61–85.

Montero, P., Talavera, C., Bea, F. 2017. Geochemical, isotopic, and zircon (U-Pb, O, Hf isotopes) evidence for the magmatic sources of the volcano-plutonic Ollo de Sapo Formation, Central Iberia. Geologica Acta 15, 245–260.

Moyes, A. B., 1993. The age and origin of the Jutulsessen granitic gneiss, Gjelsvikfjella, Dronning Maud Land. South African Journal of Antarctic Research 23, 25–32.

Moyes, A.B., Krynauw, J.R., Barton, J.M., 1995. The age of the Ritscherflya Supergroup and Borgmassivet Intrusions, Dronning Maud Land, Antarctica. Antarctic Science 7, 87–97.

Moyes, A.B., Groenewald, P.B., 1996. Isotopic constraints on Pan-African metamorphism in Dronning Maud Land, Antarctica. Chemical Geology 129, 247–256.

Murphy, J.B., Damian Nance, R., 2005. Do supercontinents turn inside-in or inside-out? International Geology Review 47, 591–619.

Nemchin, A.A., Whitehouse, M.J., Pidgeon, R.T., Meyer, C., 2006. Oxygen isotopic signature of 4.4–3.9 Ga zircons as a monitor of differentiation processes on the Moon. Geochimica et Cosmochimica Acta 70, 1864–1872.

Oriolo, S., Becker, T., 2018. The Kalahari Craton, Southern Africa: From Archean Crustal

Evolution to Gondwana Amalgamation. In: Siegesmund S., Stipp Basei M.A., Oyhantçabal P., Oriolo S. (Eds.), Geology of Southwest Gondwana, Springer International Publishing, 133–159

Palmeri, R., Godard, G., Di Vincenzo, G., Sandroni, S., Talarico, F.M., 2018. High-pressure granulite-facies metamorphism in central Dronning Maud Land (East Antarctica): implications for Gondwana assembly. Lithos 300, 361–377.

Pant, N.C., Kundu, A., D'souza, M.J., Saikia, A., 2013. Petrology of the Neoproterozoic granulites from Central Dronning Maud Land, East Antarctica–implications for southward extension of East African Orogen (EAO). Precambrian Research 227, 389–408.

Paulsson, O., Austrheim, H., 2003. A geochronological and geochemical study of rocks from Gjelsvikfjella, Dronning Maud Land, Antarctica—implications for Mesoproterozoic correlations and assembly of Gondwana. Precambrian Research 125, 113–138.

Pauly, J., Marschall, H.R., Meyer, H.P., Chatterjee, N., Monteleone, B., 2016. Prolonged Ediacaran–Cambrian metamorphic history and short-lived high-pressure granulite-facies metamorphism in the H.U. Sverdrupfjella, Dronning Maud Land (East Antarctica): evidence for continental collision during Gondwana assembly. Journal of Petrology 57,185–228.

Payne, J.L., McInerney, D.J., Barovich, K.M., Kirkland, C.L., Pearson, N.J., Hand, M., 2016. Strengths and limitations of zircon Lu-Hf and O isotopes in modelling crustal growth. Lithos 248, 175–192.

Pearce, J.A., Kempton, P.D., Nowell, G.M., Noble, S.R., 1999. Hf-Nd element and isotope perspective on the nature and provenance of mantle and subduction components in western Pacific arc-basin systems. Journal of Petrology 40, 1579–1611.

Peters, M., Haverkamp, B., Emmermann, R., Kohnen, H., Weber, K., 1991. Palaeomagnetism, K-Ar dating and geodynamic setting of igneous rocks in western and central Neuschwabenland, Antarctica. In: MRA Thomson, JA Crame, JW Thomson (Eds), Geological evolution of Antarctica, Cambridge University Press, Cambridge, 549–555.

Pisarevsky, S.A., Wingate, M.T., Powell, C.M., Johnson, S., Evans, D.A., 2003. Models of Rodinia assembly and fragmentation. Geological Society, London, Special Publication 206, 35–55.

Powell, C.M., Jones, D.L., Pisarevsky, S., Wingate, M.T.D., 2001. Palaeomagnetic constraints on the position of the Kalahari craton in Rodinia. Precambrian Research 110, 33–46.

Rehman, H.U., Kitajima, K., Valley, J.W., Chung, S.L., Lee, H.Y., Yamamoto, H., Khan, T., 2018. Low-δ^{18}O mantle-derived magma in Panjal Traps overprinted by hydrothermal alteration and Himalayan UHP metamorphism: Revealed by SIMS zircon analysis. Gondwana Research 56, 12–22.

Rivers, T., 2009. The Grenville Province as a large hot long-duration collisional orogen–insights from the spatial and thermal evolution of its orogenic fronts. Geological Society, London, Special Publication 327, 405–444.

Roberts, N.M., Spencer, C.J., 2015. The zircon archive of continent formation through time. Geological Society, London, Special Publication 389, 197–225.

Scherer, E., Münker, C., Mezger, K., 2001. Calibration of the lutetium-hafnium clock. Science 293, 683–687.

Söderlund, U., Patchett, P.J., Vervoort, J.D., Isachsen, C.E., 2004. The ^{176}Lu decay constant determined by Lu–Hf and U–Pb isotope systematics of Precambrian mafic intrusions. Earth and Planetary Science Letters 219, 311–324.

Spencer, C.J., Thomas, R.J., Roberts, N.M.W., Cawood, P.A., Millar, I., Tapster, S., 2015. Crustal growth during island arc accretion and transcurrent deformation, Natal Metamorphic Province, South Africa: New isotopic constraints. Precambrian Research 265, 203–217.

Spencer, C.J., Kirkland, C.L., Prave, A.R., Strachan, R.A., Pease, V., 2019. Crustal reworking and orogenic styles inferred from zircon Hf isotopes: Proterozoic examples from the North Atlantic region. Geoscience Frontiers 10, 417–424.
Stern, R.J., 1994. Arc assembly and continental collision in the Neoproterozoic East African Orogen: implications for the consolidation of Gondwanaland. Annual Review of Earth and Planetary Sciences 22, 319–351.
Swanson-Hysell, N.L., Kilian, T.M., Hanson, R.E., 2015. A new grand mean palaeomagnetic pole for the 1.11 Ga Umkondo large igneous province with implications for palaeogeography and the geomagnetic field. Geophysical Journal International 203, 2237–2247.
Teixeira, W., Hamilton, M.A., Lima, G.A., Ruiz, A.S., Matos, R., Ernst, R.E., 2015. Precise ID-TIMS U–Pb baddeleyite ages (1110–1112 Ma) for the Rincón del Tigre–Huanchaca large igneous province (LIP) of the Amazonian Craton: Implications for the Rodinia supercontinent. Precambrian Research 265, 273–285.
Thomas, R.J., Eglington, B.M., 1990. A Rb–Sr, Sm–Nd and U–Pb zircon isotopic study of the Mzumbe Suite, the oldest intrusive granitoid in southern Natal, South Africa. South African Journal of Geology 93, 761–765.
Thomas, R.J., Eglington, B.M., Bowring, S.A., 1993. Dating the cessation of Kibaran magmatism in Natal, South Africa. Journal of African Earth Sciences 16, 247–252.
Thomas, R.J., Agenbacht, A.L.D., Cornell, D.H., Moore, J.M., 1994. The Kibaran of southern Africa: tectonic evolution and metallogeny. Ore Geology Reviews 9, 131–160.
Thomas, R.J., Cornell, D.H., Armstrong, R.A., 1999. Provenance age and metamorphic history of the Quha Formation, Natal Metamorphic Province: A U-Th-Pb zircon SHRIMP study. South African Journal of Geology 102, 83–88.
Thomas, R.J., Jacobs, J., Eglington, B.M., 2000. Geochemistry and isotopic evolution of the Mesoproterozoic Cape Meredith Complex, West Falkland. Geological Magazine 137, 537–553.
Thomas, R.J., Armstrong, R.A. Eglington, B.M., 2003. Geochronology of the Sikombe Granite, Transkei, Natal Metamorphic Province, South Africa. South African Journal of Geology 106, 403–408.
Thomas, R.J., Jacobs, J., Horstwood, M.S.A., Ueda, K., Bingen, B., Matola, R., 2010. The Mecubúri and Alto Benfica groups, NE Mozambique: Aids to unravelling ca. 1 and 0.5 Ga events in the east African orogen. Precambrian Research 178, 72–90.
Valley, J.W., Kinny, P.D., Schulze, D.J., Spicuzza, M.J., 1998. Zircon megacrysts from kimberlite: oxygen isotope variability among mantle melts. Contributions to mineralogy and petrology 133, 1–11.
Valley, J.W., 2003. Oxygen isotopes in zircon. Reviews in Mineralogy and Geochemistry 53, 343–385.
Vroon, P.Z., Lowry, D., van Bergen, M.J., Boyce, A.J., Mattey, D.P., 2001. Oxygen isotope systematics of the Banda Arc: low δ18O despite involvement of subducted continental material in magma genesis. Geochimica et Cosmochimica Acta 65, 589–609.
Wareham, C.D., Pankhurst, R.J., Thomas, R.J., Storey, B.C., Grantham, G.H., Jacobs, J., Eglington, B.M., 1998. Pb, Nd, and Sr isotope mapping of Grenville-age crustal provinces in Rodinia. The Journal of Geology 106, 647–660.
Weil, A.B., Van der Voo, R., Mac Niocaill, C., Meert, J.G., 1998. The Proterozoic supercontinent Rodinia: paleomagnetically derived reconstructions for 1100 to 800 Ma. Earth and Planetary science letters 154, 13–24.
Wiedenbeck, M., Hanchar, J.M., Peck, W.H., Sylvester, P., Valley, J., Whitehouse, M., Kronz, A., Morishita, Y., Nasdala, L., Fiebig, J., Franchi, I., 2004. Further characterisation of the 91500 zircon crystal. Geostandards and Geoanalytical Research 28, 9–39.

Woodhead, J.D., Hergt, J.M., 2005. A preliminary appraisal of seven natural zircon reference materials for in situ Hf isotope determination. Geostandards and Geoanalytical Research 29, 183–195.

Wolmarans, L.C., Kent, K.E., 1982. Geological investigations in western Dronning Maud Land, Antarctica — a synthesis. South African Journal of Antarctic Research (Supplements 2).

Zheng, Y.F., Wu, Y.B., Chen, F.K., Gong, B., Li, L., Zhao, Z.F., 2004. Zircon U-Pb and oxygen isotope evidence for a large-scale ^{18}O depletion event in igneous rocks during the Neoproterozoic. Geochimica et Cosmochimica Acta 68, 4145–4165.